NON-EQUILIBRIUM TRIBLOCK TERPOLYMER STRUCTURES AS ULTRAFILTRATION MEMBRANES

A Dissertation

Presented to the Faculty of the Graduate School

of Cornell University

In Partial Fulfillment of the Requirements for the Degree of

Doctor of Philosophy

by

Rachel Mika Dorin

May 2013

NON-EQUILIBRIUM TRIBLOCK TERPOLYMER STRUCTURES AS ULTRAFILTRATION MEMBRANES

Rachel Mika Dorin, Ph. D.

Cornell University 2013

Block copolymers are promising as materials for ultrafiltration membranes due to their ability to self-assemble into periodic, ordered structures on length scales of ~5-50 nm. Most efforts towards fabricating functional membranes from block copolymers have targeted equilibrium morphologies, which may results in a number of potential disadvantages, including a lack of porosity in the as made films, thick separation layers, or tedious transfer and post-functionalization steps. In this dissertation, non-equilibrium block copolymer structures are used in the fabrication of ultrafiltration membranes. A system containing the triblock terpolymer poly(isoprene-*b*-styrene-*b*-4-vinyl pyridine) and the solvents 1,4-dioxane and tetrahydrofuran is studied in detail. Ultrafiltration membranes fabricated from this system using a combination of self-assembly and non-solvent induced phase separation are shown to have a thin, isoporous separation layer above an asymmetric substructure. The structure and performance of these membranes are characterized using techniques such as electron microscopy, permeability, and solute rejection. The formation mechanism of the non-equilibrium triblock terpolymer membranes is studied using small angle X-ray scattering and grazing incidence small-angle X-ray scattering techniques.

BIOGRAPHICAL SKETCH

The fourth of five children, Rachel Mika Dorin was born in Mountain View, California to Richard and Maxine Dorin. Foreshadowing a tendency for the dramatic, Rachel decided to enter the world while Rick and Maxine were enjoying the movie *Romancing the Stone* in a theater. Born on the fourth of July, Rachel has since been known as the firecracker in her family.

After a year in Kyoto, Japan at the age of three, Rachel moved with her family to Albuquerque, New Mexico, where she attended middle and high school at Albuquerque Academy. She started her collegiate career as a banana slug at the University of California, Santa Cruz, transferring to her hometown school, the University of New Mexico, two years later. At UNM Rachel majored in both Chemistry and Biology, and joined the Shelnutt group at Sandia National Labs. At the labs, Rachel worked for three years under the supervision of Dr. Yujiang Song. It was there that Rachel developed an affinity for research and science, and the lab experience proved transformative for her career, inspiring applications to PhD programs in Materials Science across the country.

For her PhD research, Rachel moved to Ithaca, NY, home to Cornell University, in 2008. She quickly became enamored with the college-town environment, despite the cold winters. Shortly after arriving in Ithaca, Rachel also became enamored with one John DeFranco, a senior graduate student working in the same department. After dating for several years and recognizing their shared dreams, the two were married on September 29, 2012 on a bluff in Pacific Grove, California. While her experience at Cornell was overwhelmingly positive, meeting John was the best things about it.

At Cornell, Rachel joined the Wiesner research group, studying block copolymer self-assembly and their application to membranes, the topic of this

dissertation. Minoring in business and leading the technology entrepreneurship club generated a strong desire in Rachel to learn skills beyond the lab and bridge the gap between science and business. She is looking forward to starting a company based on her research after graduating and continuing her journey of personal development.

To John, whose friendship, love, and support have brightened my life

ACKNOWLEDGMENTS

There are many groups and individuals both at the University and beyond to whom I am grateful. First, I would like to thank my PhD advisor, Professor Ulrich Wiesner. His scientific expertise and technical advice over the course of my program has been invaluable. To my special committee members, Professors Christopher Ober and David BenDaniel, thank you for the research and business advice and support.

I am indebted to the support of the entire Wiesner research group, including but not limited to my friends and colleagues Zihui Li, Kahyun Hur, Srikant Iyer, Kwan Wee Tan, Christina Cowman-Eggert, Spencer Robbins, Patrick Boldrighini, Morgan Stefik, and my undergrad Deborah Liu. Sincere appreciation goes out especially to Dr. Yujiang Song for his professional guidance, and to Hiroaki Sai for teaching me to make my first polymer and for his kind and generous expertise over the past five years. Thank you to Joerg Werner for helping me struggle through the first year of making membranes, and gratitude to Professor William Phillip, whose partnership in research and guidance in writing my first paper was critical to my success.

Finally, to my family, I could not have made it to today without your unwavering support. All my love and appreciation to my parents, Maxine and Richard, my siblings, Randy, Faie, Philip, and Katie, my grandparents, Robert and Shirley, and my dear husband, John.

TABLE OF CONTENTS

LIST OF FIGURES

LIST OF TABLES

LIST OF ABBREVIATIONS

FFT – Fast Fourier transform

GISAXS – Grazing incidence small-angle X-ray scattering

ISV – Poly(isoprene-*b*-styrene-*b*-4-vinyl pyridine)

PI-*b*-PS-*b*-P4VP - Poly(isoprene-*b*-styrene-*b*-4-vinyl pyridine)

PS-*b*-PMMA – Poly(styrene-*b*-methyl methacrylate)

PS-*b*-PEO – Poly(styrene-*b*-ethylene oxide)

PS-*b*-P2VP – Poly(styrene-*b*-2-vinyl pyridine)

PS-*b*-P2VP-*b*-PEO – Poly(styrene-*b*-2-vinyl pyridine-*b*-ethylene oxide)

PS-*b*-P4VP – Poly(styrene-*b*-4-vinyl pyridine)

SAXS – Small-angle X-ray Scattering

SEM – Scanning electron microscopy

SNIPS – Self-assembly and non-solvent induced phase separation

TEM – Transmission electron microscopy

CHAPTER 1

Introduction

The spontaneous organization of distinct building blocks into patterned structures, known as self-assembly, occurs on length scales ranging from angstroms to millimeters and larger.[1] Naturally occurring self-assembly, for example molecular recognition in nucleic acid chains, secondary, tertiary, and quaternary protein structures, and bacteriophage bodies, illuminates methods for applying self-organization to synthetic systems.[2] Such methods may provide pathways to materials with novel and advantageous property profiles.

1.1 Block Copolymer Self-Assembly

Block copolymers can be used to address self-assembled systems at mesoscopic length scales. Block copolymers are macromolecules composed of two or more chemically distinct polymer subunits covalently bonded together. The mixing of two polymer species A and B can be understood through the Flory-Huggins treatment in which the change in the free energy of mixing, ΔG_{mix}, is calculated by:

$$\Delta G_{mix} = k_B T\left[N_A \ln f_A + N_B \ln f_B + \chi_{AB} N_A f_B\right] \tag{1}$$

where k_B is the Boltzmann constant, T is the temperature, N_i is the number of polymer chains i, f_i is the volume fraction of polymer i, and χ_{ij} is the Flory-Huggins interaction parameter between polymers i and j.[3] Polymer mixing is favorable when $\Delta G_{mix} < 0$, while polymer phase separation occurs when $\Delta G_{mix} > 0$. The Flory-Huggins interaction parameter between monomers A and B, χ_{AB}, can be determined by a lattice model:

$$\chi_{AB} = \left(\frac{z}{k_B T}\right)\left[\varepsilon_{AB} - \frac{1}{2}\left(\varepsilon_{AA} + \varepsilon_{BB}\right)\right] \tag{2}$$

where z is the coordination number, and $-\varepsilon_{ij}$ are the attractive non-bonded nearest neighbor van der Waals interaction energies.[4] χ_{AB} can also be practically estimated using contributions to the Hansen solubility parameter as:

$$\chi_{AB} = \frac{V_m}{k_B T}\left[\left(\delta_{dA} - \delta_{dB}\right)^2 + 0.25\left(\delta_{pA} - \delta_{pB}\right)^2 + 0.25\left(\delta_{hA} - \delta_{hB}\right)^2\right] \quad (3)$$

where V_m is the molar volume, δ_{di} is the dispersive, δ_{pi} is the polar, and δ_{hi} is the hydrogen bonding contribution of polymer *i* to the Hansen solubility parameter.[5] When χ_{AB} is sufficiently positive and the value of $\chi_{AB}N$ is sufficiently large, phase separation occurs. In block copolymer systems, the covalent bond connecting neighboring polymer blocks results in microphase separation and the formation of periodic, ordered structures with length scales ranging from ~5-100 nm. Typical diblock copolymer morphologies include the spherical body-centered cubic micelle (S, S'), hexagonal rod (H, H'), gyroid (G, G'), and lamellar (L) phases. Phase diagrams for block copolymers plotting $\chi_{AB}N$, where N is the overall degree of polymerization of the polymer, is plotted against the volume fraction of polymer A, f_A, can be used to visualize the morphologies of block copolymers of various compositions. An example of a theoretical phase diagram for a diblock copolymer is shown in Figure 1.1.[6]

1.2 Block Copolymer-Derived Membrane Materials

Over the past two decades, researchers attempting to improve membrane-based separations have increasingly looked to block copolymer self-assembly to solve the performance limitations of current membrane technologies. The typical length scale of block copolymer self-assembly makes block copolymer membranes particularly applicable to ultrafiltration, which can be used in, for example, biopharmaceutical

processing, water and wastewater pretreatment, and nutraceuticals, which are substances purified from food products. The combination of high pore densities with uniform pore diameters achievable with block copolymer-based membranes provides opportunities to significantly improve both permeability and selectivity. Several techniques for fabricating such membranes have been developed, including spin coating, bulk casting, and self-assembly combined with phase-separation.

Functional membranes fabricated by spin coating block copolymer thin films was first demonstrated by Yang *et al.* in which a thin film of PS-*b*-PMMA diblock copolymer mixed with PMMA homopolymer was spin-coated onto a silicon wafer.[7] Subsequent efforts on spin coated membranes resulted in improved chemical and mechanical resistance,[8-10] as well as their use in controlled-release drug delivery.[11] While the spin-coating method results in functional membranes, tedious transfer steps are often necessary. Furthermore, typically one block must be removed to convey porosity, and large area membranes are difficult to produce.

A second method for preparing block copolymer membranes is through bulk casting. Examples of this method include doctor blading of block copolymer solutions onto porous supports,[12] drop-casting on non-porous substrates,[13-15] and block copolymer melt extrusion.[16] While functional membranes can be produced using bulk casting, this technique typically results in membranes that are a minimum of tens of microns thick, leading to low fluxes.

A recently developed method[17] known as self-assembly and non-solvent induced phase separation, or SNIPS,[18] advances the practical application of block copolymer membranes in that it is both industrially scalable and produces membranes

with thin selective layers. The SNIPS technique involves doctor blading a block copolymer solution onto a substrate, allowing the film to evaporate for a specified period of time, and plunging the entire film into a non-solvent bath. During the evaporation period, as the solvent at the film/air interface depletes, the block copolymer begins to self-assemble. During the plunging step, the casting solvents and non-solvent mix, causing the polymer to precipitate. A schematic of this procedure is shown in Figure 1.2. SNIPS yields a uniformly isoporous separation layer ~100 nm in thickness above an asymmetric, spongy support ~ 50 μm in thickness.

The SNIPS method was first demonstrated with the diblock copolymer PS-*b*-P4VP in 2007 by Peinemann *et al.*[17] The method was translated to triblock terpolymers using PI-*b*-PS-*b*-P4VP, which improved mechanical strength and expanded the range of possible chemical compositions.[19] Due to the impressive flux and rejection characteristics demonstrated by SNIPS membranes, the focus of subsequent efforts have been twofold: 1) elucidating the underlying mechanism that results in isoporous materials and 2) increasing chemical and physical functionality. Studies to understand the SNIPS formation mechanism to date have included small-angle X-ray scattering on casting solutions[18], small-angle neutron scattering,[20] cryo-transmission electron microscopy,[20, 21] cryo-scanning electron microscopy,[20-22] and transmission electron microscopy tomography.[23] Research towards advancing chemical and physical functionality of SNIPS membranes has produced a small library of possible block copolymers, including PS-*b*-P2VP,[24] PS-*b*-PEO,[25] and PS-*b*-P2VP-*b*-PEO.[26] Tuning pore size through molecular design,[27] small molecule additives,[28] polymer additives,[19] and post-functionalization[29] have been demonstrated as methods

for developing SNIPS membranes for a broad application of membrane-based separations.

This dissertation focuses on both understanding the mechanism of formation and advancing the chemical and physical properties of SNIPS membranes. In the first part, demonstration of the SNIPS process with a triblock terpolmer, PI-*b*-PS-*b*-P4VP, is described. Next, small-angle X-ray scattering studies on block copolymer solutions is used as a predictive tool for SNIPS membrane formation and structure. In a subsequent chapter molecular block copolymer architecture-membrane structure and performance correlations are elucidated. Finally, *in situ* grazing incidence small-angle X-ray scattering during the SNIPS process reveals details of the membrane formation process.

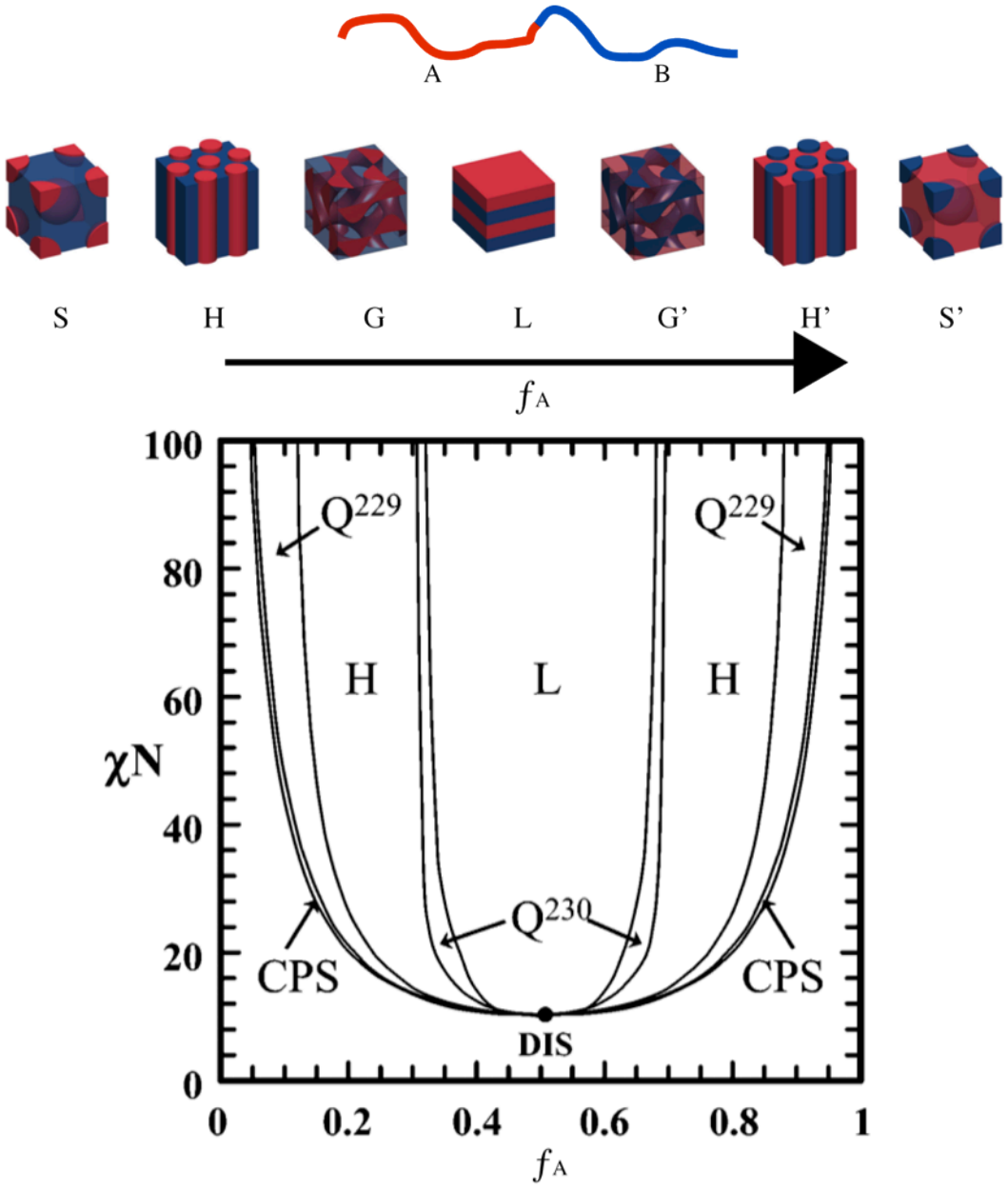

Figure 1.1 Schematics of a block copolymer and typical block copolymer morphologies (top) and theoretical phase diagram of an idealized diblock copolymer (bottom).[6]

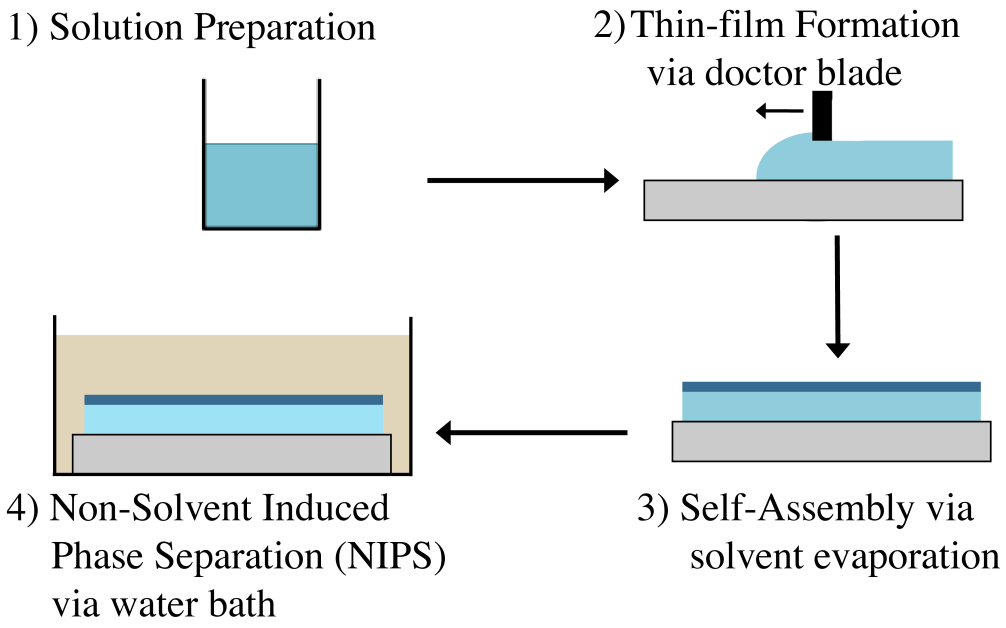

Figure 1.2 Schematic of the SNIPS method for fabricating membranes in four steps: In step one, a casting dope is prepared by dissolving a block copolymer in organic solvents. Step two involves doctoring blading the casting solution onto a substrate. In step three, the cast film is allowed to evaporated for a specific period of time, allowing the top surface to self-assemble and form the isoporous separation layer. Finally, the entire film, including the substrate, is plunged into a non-solvent bath, solidifying the polymer and producing an asymmetric, supportive substructure to the separation layer.

REFERENCES

1. Whitesides, G. M.; Grzybowski, B., Self-Assembly at All Scales. *Science* **2002,** *295* (5564), 2418-2421.

2. Philp, D.; Stoddart, J. F., Self-Assembly in Natural and Unnatural Systems. *Angewandte Chemie International Edition in English* **1996,** *35* (11), 1154-1196.

3. Flory, P. J., *Principles of polymer chemistry*. Cornell University Press: Ithaca, 1953.

4. Freed, K. F., New lattice model for interacting, avoiding polymers with controlled length distribution. *Journal of Physics A: Mathematical and General* **1985,** *18* (5), 871.

5. Hansen, C. M., *Hansen Solubility Parameters: A User's Handbook*. 2nd ed.; CRC Press: Boca Raton, FL, 2007.

6. Cochran, E. W.; Garcia-Cervera, C. J.; Fredrickson, G. H., Stability of the Gyroid Phase in Diblock Copolymers at Strong Segregation. *Macromolecules* **2006,** *39* (7), 2449-2451.

7. Yang, S. Y.; Ryu, I.; Kim, H. Y.; Kim, J. K.; Jang, S. K.; Russell, T. P., Nanoporous Membranes with Ultrahigh Selectivity and Flux for the Filtration of Viruses. *Advanced Materials* **2006,** *18* (6), 709-712.

8. Yang, S. Y.; Park, J.; Yoon, J.; Ree, M.; Jang, S. K.; Kim, J. K., Virus Filtration Membranes Prepared from Nanoporous Block Copolymers with Good Dimensional Stability under High Pressures and Excellent Solvent Resistance.

Advanced Functional Materials **2008,** *18* (9), 1371-1377.

9. Li, X.; Fustin, C.-A.; Lefevre, N.; Gohy, J.-F.; Feyter, S. D.; Baerdemaeker, J. D.; Egger, W.; Vankelecom, I. F. J., Ordered nanoporous membranes based on diblock copolymers with high chemical stability and tunable separation properties. *Journal of Materials Chemistry* **2010,** *20* (21), 4333-4339.

10. Yamamoto, T.; Kimura, T.; Komura, M.; Suzuki, Y.; Iyoda, T.; Asaoka, S.; Nakanishi, H., Block Copolymer Permeable Membrane with Visualized High-Density Straight Channels of Poly(ethylene oxide). *Advanced Functional Materials* **2011,** *21* (5), 918-926.

11. Yang, S. Y.; Yang, J.-A.; Kim, E.-S.; Jeon, G.; Oh, E. J.; Choi, K. Y.; Hahn, S. K.; Kim, J. K., Single-File Diffusion of Protein Drugs through Cylindrical Nanochannels. *ACS Nano* **2010,** *4* (7), 3817-3822.

12. Phillip, W. A.; O'Neill, B.; Rodwogin, M.; Hillmyer, M. A.; Cussler, E. L., Self-Assembled Block Copolymer Thin Films as Water Filtration Membranes. *ACS Applied Materials & Interfaces* **2010,** *2* (3), 847-853.

13. Chen, L.; Phillip, W. A.; Cussler, E. L.; Hillmyer, M. A., Robust Nanoporous Membranes Templated by a Doubly Reactive Block Copolymer. *Journal of the American Chemical Society* **2007,** *129* (45), 13786-13787.

14. Phillip, W. A.; Amendt, M.; O,ÄôNeill, B.; Chen, L.; Hillmyer, M. A.; Cussler, E. L., Diffusion and Flow Across Nanoporous Polydicyclopentadiene-Based Membranes. *ACS Applied Materials & Interfaces* **2009,** *1* (2), 472-480.

15. Li, L.; Schulte, L.; Clausen, L. D.; Hansen, K. M.; Jonsson, G. E.; Ndoni, S., Gyroid Nanoporous Membranes with Tunable Permeability. *ACS Nano* **2011,** *5* (10),

7754-7766.

16. Phillip, W. A.; Rzayev, J.; Hillmyer, M. A.; Cussler, E. L., Gas and water liquid transport through nanoporous block copolymer membranes. *Journal of Membrane Science* **2006,** *286* (1,Äì2), 144-152.

17. Peinemann, K. V.; Abetz, V.; Simon, P. F., Asymmetric superstructure formed in a block copolymer via phase separation. *Nat Mater* **2007,** *6* (12), 992-6.

18. Dorin, R. M.; Marques, D. S.; Sai, H.; Vainio, U.; Phillip, W. A.; Peinemann, K.-V.; Nunes, S. P.; Wiesner, U., Solution Small-Angle X-ray Scattering as a Screening and Predictive Tool in the Fabrication of Asymmetric Block Copolymer Membranes. *ACS Macro Letters* **2012,** *1* (5), 614-617.

19. Phillip, W. A.; Mika Dorin, R.; Werner, J.; Hoek, E. M. V.; Wiesner, U.; Elimelech, M., Tuning Structure and Properties of Graded Triblock Terpolymer-Based Mesoporous and Hybrid Films. *Nano Letters* **2011,** *11* (7), 2892-2900.

20. Oss-Ronen, L.; Schmidt, J.; Abetz, V.; Radulescu, A.; Cohen, Y.; Talmon, Y., Characterization of Block Copolymer Self-Assembly: From Solution to Nanoporous Membranes. *Macromolecules* **2012,** *45* (24), 9631-9642.

21. Nunes, S. P.; Sougrat, R.; Hooghan, B.; Anjum, D. H.; Behzad, A. R.; Zhao, L.; Pradeep, N.; Pinnau, I.; Vainio, U.; Peinemann, K.-V., Ultraporous Films with Uniform Nanochannels by Block Copolymer Micelles Assembly. *Macromolecules* **2010,** *43* (19), 8079-8085.

22. Nunes, S. P.; Karunakaran, M.; Pradeep, N.; Behzad, A. R.; Hooghan, B.; Sougrat, R.; He, H.; Peinemann, K.-V., From Micelle Supramolecular Assemblies in Selective Solvents to Isoporous Membranes. *Langmuir* **2011,** *27* (16), 10184-10190.

23. Nunes, S. P.; Behzad, A. R.; Hooghan, B.; Sougrat, R.; Karunakaran, M.; Pradeep, N.; Vainio, U.; Peinemann, K.-V., Switchable pH-Responsive Polymeric Membranes Prepared via Block Copolymer Micelle Assembly. *ACS Nano* **2011,** *5* (5), 3516-3522.

24. Jung, A.; Rangou, S.; Abetz, C.; Filiz, V.; Abetz, V., Structure Formation of Integral Asymmetric Composite Membranes of Polystyrene-block-Poly(2-vinylpyridine) on a Nonwoven. *Macromolecular Materials and Engineering* **2012,** *297* (8), 790-798.

25. Hahn, J.; Filiz, V.; Rangou, S.; Clodt, J.; Jung, A.; Buhr, K.; Abetz, C.; Abetz, V., Structure formation of integral-asymmetric membranes of polystyrene-block-Poly(ethylene oxide). *Journal of Polymer Science Part B: Polymer Physics* **2013,** *51* (4), 281-290.

26. Jung, A.; Filiz, V.; Rangou, S.; Buhr, K.; Merten, P.; Hahn, J.; Clodt, J.; Abetz, C.; Abetz, V., Formation of Integral Asymmetric Membranes of AB Diblock and ABC Triblock Copolymers by Phase Inversion. *Macromolecular Rapid Communications* **2013**, DOI: 10.1002/marc.201200770.

27. Dorin, R. M.; Phillip, W. A.; Sai, H.; Werner, J.; Elimelech, M.; Wiesner, U., Designing Block Copolymer Architectures for Targeting Membrane Performance. *ACS Nano* **2013,** *Submitted*.

28. Clodt, J. I.; Rangou, S.; Schröder, A.; Buhr, K.; Hahn, J.; Jung, A.; Filiz, V.; Abetz, V., Carbohydrates as Additives for the Formation of Isoporous PS-b-P4VP Diblock Copolymer Membranes. *Macromolecular Rapid Communications* **2013,** *34* (2), 190-194.

29. Clodt, J. I.; Filiz, V.; Rangou, S.; Buhr, K.; Abetz, C.; Höche, D.; Hahn, J.; Jung, A.; Abetz, V., Double Stimuli-Responsive Isoporous Membranes via Post-Modification of pH-Sensitive Self-Assembled Diblock Copolymer Membranes. *Advanced Functional Materials* **2012,** *23* (6), 731-738.

CHAPTER 2

Tuning Structure and Properties of Graded Triblock Terpolymer-Based Mesoporous and Hybrid Films*

Abstract

Despite considerable efforts towards fabricating ordered, water-permeable, mesoporous films from block copolymers, fine control over pore dimensions, structural characteristics, and mechanical behavior of graded structures remains a major challenge. To this end, we describe the fabrication and performance characteristics of graded mesoporous and hybrid films derived from the newly synthesized triblock terpolymer, poly(isoprene-*b*-styrene-*b*-4-vinylpyridine). A unique morphology, unachievable in diblock copolymer systems, with enhanced mechanical integrity is evidenced. The film structure comprises a thin selective layer containing vertically aligned and nearly monodisperse mesopores at a density of more than 10^{14} pores/m^2 above a graded macroporous layer. Hybridization via homopolymer blending enables tuning of pore size within the range of 16 to 30 nm. Solvent flow and solute separation experiments demonstrate that the terpolymer films have permeabilities comparable to commercial membranes, are stimuli-responsive, and contain pores with a nearly monodisperse diameter. These results suggest that moving to multiblock polymers and their hybrids may open new paths to produce high performance graded

* Reproduced with permission from Phillip, W. A.; Mika Dorin, R.; Werner, J.; Hoek, E. M. V.; Wiesner, U.; Elimelech, M., Tuning Structure and Properties of Graded Triblock Terpolymer-Based Mesoporous and Hybrid Films. *Nano Letters* **2011,** *11* (7), 2892-2900. Copyright 2011 American Chemical Society.

membranes for filtration, separations, nanofluidics, catalysis, and drug delivery.

Keywords: Triblock Terpolymer, Self-assembly, Mesoporous, Membranes, Polyisoprene-*b*-polystyrene-*b*-poly-4-vinyl pyridine, Filtration

Understanding and controlling the transport of chemical species at the nanoscale will enable the design of novel devices and systems capable of addressing several of the issues facing chemical separations (e.g., water purification[1] and bioseparations[2]), drug delivery, and molecular sensing.[3] Many of these technologies will rely on a membrane or thin film with robust mechanical properties and well-controlled pore dimensions and chemistries. In order to advance the understanding and implementation of technologies that exploit transport phenomena at the nanoscale, it is essential to make progress towards fabrication and characterization of next generation, high performance mesoporous materials.

One promising route to major improvements in this research area is the formation of mesoporous and hybrid films through block copolymer self-assembly.[4, 5] Block copolymers—an intriguing class of macromolecules known to microphase separate into periodic, ordered structures with length scales typically ranging from 5 to 50 nm—offer a functional approach for designing a versatile assortment of mesoscale hybrid materials, such as patterned media[6, 7] and devices, including batteries,[8, 9] solar cells,[10, 11] and fuel cells.[12] In addition to applications in drug delivery and nanofluidics, copolymer-derived mesoporous films are strong candidates as highly selective separation membranes.

Membranes based on diblock copolymer and triblock terpolymer self-assembly

have been generated through bulk casting, but these non-graded materials suffer from low permeabilities due to relatively thick selective layers, and hybrids were not investigated.[13-16] Mesoporous thin films from diblock copolymers have been fabricated by spin coating onto solid substrates; however, this method requires long annealing times and the tedious transfer of a fragile thin film from the primary substrate to a secondary support membrane.[17-20] A third approach combines the self-assembly of diblock copolymers with non-solvent induced phase separation; however, a thorough performance evaluation of the resulting membranes has not yet been attempted, and the use of glassy diblock copolymers in this system reduces the opportunity for chemical and mechanical tunability.[21, 22]

Here we describe the facile and scalable fabrication of novel, graded, ABC-type triblock terpolymer-derived mesoporous films, and elucidate the benefits of utilizing a multiblock polymer system. The structural and performance characteristics of the mesoporous films, including both stimuli responsive permeation and separation, are shown. Pore size tunability through simple hybridization via polymer blending and the subsequent effect on separation performance is reported. These films, which contain more than 10^{14} pores/m^2, have permeabilities comparable to commercial ultrafiltration membranes, while producing solute separations consistent with films containing monodisperse mesopores.

A novel triblock terpolymer, poly(isoprene-*b*-styrene-*b*-4-vinylpyridine) (ISV), was synthesized by anionic polymerization as the starting material for the formation of the graded mesoporous films described herein. A detailed description of the synthetic procedure can be found in Appendix A. Figure 2.1a shows the chemical structure of

the terpolymer together with a table of the polymer-solvent interaction parameters, χ_{1-2}, for the different solvents used here, as calculated from solubility parameters.[23] The material used in this study, referred to as ISV-77, had a total molar mass of 76.6 kg/mol, a polydispersity of 1.16, and volume fractions of 0.29, 0.56, and 0.15 for the polyisoprene (PI), polystyrene (PS), and poly-4-vinylpyridine (P4VP) domains, respectively. Figure 2.1b shows both a small angle X-ray scattering (SAXS) trace and a transmission electron microscopy (TEM) micrograph of a bulk ISV-77 film cast from chloroform, both of which are consistent with a hexagonally close packed cylinder morphology, where P4VP forms the cylinder cores.

In order to get an impression of the mechanical response of this material relative to a diblock copolymer of similar molecular characteristics, Figure 2.1c compares representative stress strain curves for bulk ISV-77 and a bulk poly(styrene-*b*-4-vinylpyridine) (SV) sample with hexagonal P4VP cylinder morphology (data not shown). The SV diblock molar mass was 56 kg/mol with polydispersity of 1.19, and volume fractions of 0.71 and 0.29 for PS and P4VP, respectively. The area under the ISV-77 curve, representing the toughness of the material, is 9.0 GJ/m^3, almost triple that of the 3.20 GJ/m^3 toughness of the glassy SV, which can be attributed to the addition of the rubbery, low T_g polyisoprene domain[24]. The results of these tensile tests suggest that the ISV polystyrene domains are interconnected, which is evidenced by a more careful look at the morphology of this cast material (inset in Figure 2.1b). This simple bulk comparison demonstrates the potential for tuning the mechanical response of mesostructured materials by moving from diblock to multiblock systems.[25] Other advantages include the expanded phase space over which triblock

terpolymers and other multiblock systems exhibit bicontinuous morphologies, which have been shown to exhibit enhanced mechanical properties due to the continuity of multiple domains,[26, 27] as well as additional control over chemical functionality.[4]

The graded, mesoporous terpolymer films are formed using a combination of controlled solvent evaporation and non-solvent induced phase separation[28] (NIPS). The solvent evaporation directs the self-assembly of the terpolymer to template the structure of the mesoporous selective layer, and the subsequent NIPS process creates the underlying macroporous support structure. A vast parameter range was screened to find appropriate film formation conditions. The protocol for casting a film begins by dissolving the ISV in an appropriate solvent. This solvent must fulfill two requirements; it must result in the desired orientation of self-assembled morphology at the top surface of the film upon evaporation,[29] and it must be miscible with the non-solvent for the NIPS process. From the large library of possible solvents, we found that a mixture of 1,4-dioxane/tetrahydrofuran (70/30 by weight) fulfilled both these requirements.

A 12 wt% polymer solution was drawn into a film on a glass substrate using a doctor's blade set at a gate height of 225 μm. After the film was cast, the solvent was allowed to evaporate for a predetermined period of time, during which the concentration of polymer at the air/film interface increased. The film was subsequently plunged into a non-solvent (water) bath, causing the precipitation of the underlying polymer into an asymmetric macroporous structure. The selection of polymer concentration, substrate, and gate height all affect the ultimate macro- and meso-structure of the resulting film, and were carefully optimized. For example, low

polymer concentrations (<10 wt%) resulted in low polymer connectivity upon plunging in the non-solvent, while a hydrophobic Teflon substrate caused the film to de-wet. A large gate height (>400 μm) yielded cracks in the film due to instabilities at the free surface.

Scanning electron microscopy (SEM) micrographs of the cross-section of ISV-77 films are shown at different magnifications in Figure 2.2a and b, and display the asymmetric structure that results from the protocol described above. The film is densest at the top surface of the film where the polymer concentration was highest prior to beginning the NIPS process. The substructure pores increase in size and the film becomes more open towards the bottom surface. Sheets of 40-μm-thick ISV-77 mesoporous films as large as 300 cm^2 were fabricated in the lab for permeability and solute separation testing. This fabrication method has the important benefit of industrial scalability.[30]

The length of the solvent evaporation step is another process variable that significantly affects the final structure of the film. Specifically, the solvent evaporation step is critical to directing the self-assembly of the terpolymer. Solvent evaporation into the open atmosphere created fast evaporation conditions, which can be used to orient the cylindrical domains perpendicular to the thin dimension of the film.[16, 29, 31] Figure 2.3 shows SEM micrographs of the top surface of films cast under identical conditions, but with solvent evaporation times of 15, 30, 45, and 75 s. These micrographs elucidate the film structure dependence on the length of the evaporation step. For short evaporation times (i.e., 15 and 30 s), the local concentration of polymer was not high enough to form a dense skin layer. Thus, when the film was plunged into

the water bath, a macroporous structure resulted even at the surface. Open network structures formed when an evaporation time of 15 s was used, while at 30 s dense regions were observed with pores 50-200 nm in diameter randomly distributed across the surface. The film cast using a 45 s evaporation period had a dense skin layer, but only a few nanopores began to nucleate at the surface. Allowing the solvent to evaporate for 75 s produced the desired nanostructure—a selective skin layer containing a high density of nanopores ~20 nm in diameter. The narrow pore size distribution suggests that their structure is a result of the triblock terpolymer self-assembly.

Cross sections of the self-assembled surface structure are readily visualized by transmission and scanning electron microscopy (Figure 2.4a-c). Figures 2.4a and b show TEM micrographs of films selectively stained with OsO_4 (PI selective stain) and I_2 (P4VP selective stain), respectively. In Figure 2.4a, the circular dark regions, which appear cubically-packed at the top, correspond to the stained PI of the terpolymer. This intriguing structure is reminiscent of high impact polystyrene (HIPS), in which rubbery inclusions act to dissipate stress from the glassy PS surrounding it. Indeed, this affords the film increased resistance against fracture,[32] which makes handling of these membranes much easier than membranes derived from SV diblock copolymers (Figure 2.1c). In Figure 2.4b, the P4VP domains appear as the dark lines running vertically through the film. These domains are consistent with the mesopores running from the top surface into the underlying macroporous support, as corroborated by the SEM micrograph in Figure 2.4c. These channels act as highly uniform mesopores through which gases or liquids can be transported, and potentially separated.

Interestingly, closer examination of the mesopores on the top surface of the terpolymer film reveals that their packing is in a square lattice rather than in a hexagonal array, as seen in the equilibrium bulk morphology. Figure 2.4d shows a radially integrated FFT of an SEM micrograph of the top surface where indices consistent with a square packed lattice are marked. From this data, a pore d-spacing of 44 nm and an areal pore density of 5.2×10^{14} pores/m^2 can be calculated.

The results above demonstrate our ability to fabricate large areas of mesoporous films containing a high density of nearly monodisperse pores. The unique kinetically-trapped structure of the films can be further studied by measuring transport properties, such as the permeability to liquids or gases and the ability to selectively separate dissolved solutes. These experiments not only provide more insight into the nanostructure of the film, but are also critical to examining the utility of the films in membrane filtration, drug delivery, and sensing applications.

Results of flow experiments conducted with acetate buffer solutions between pH 4 and 6 are shown in Figure 2.5a; the hydraulic permeability of the films was a strong function of pH. At pH 5 and higher, there was a small increase in permeability with increasing pH. Below a pH of 5, the permeability decreased rapidly, reaching a value of 2.2 L $m^{-2}hr^{-1}bar^{-1}$ at pH 4, nearly 80 times lower than the permeability at pH 6 of 160 L $m^{-2}hr^{-1}bar^{-1}$.

The stimuli responsive permeability provides evidence that the mesopores are coated with a P4VP brush,[33, 34] consistent with the micrographs in Figures 2.3 and 2.4. P4VP has a pKa of 4.6, which is near the pH where our films become pH responsive. At pH values below the pKa, the degree of protonation of the P4VP is higher, making

it more soluble in the aqueous buffer solutions. The better solvated P4VP extends toward the center of the pore, slowing the flow of the aqueous solution. Conversely, deprotonated P4VP is not well solvated by the solutions and retracts against the pore walls to open the pores to flow. Similar results were obtained using a 50/50 (w/w) solution of ethanol/DI. In the presence of ethanol, which is a good solvent for P4VP, the permeability decreases to values similar to that at pH 4. These results suggest that it is the solvent quality for P4VP that results in the stimuli responsive nature of the films.

Solute separation (rejection) tests are a similarly valuable tool for exploring the structure of the mesoporous films, and critical to confirming an absence of defects. Single solute PEO samples dissolved in DI and ranging in molar mass from 4 to 203 kg/mol were used to challenge the films. Observed percent rejections were calculated by comparing the PEO concentration in the permeate and feed solutions. Results from these experiments are shown as open circles in Figure 2.5b. As the PEO molar mass increases, the percent rejection also increases. For example, a 10 kg/mol sample was only slightly rejected (~18% rejection) while a 95 kg/mol sample was almost completely rejected (~95% rejection).

The solute rejection data can be used to estimate the pore size of the film. However, it is important to ensure the calculation of an intrinsic film property, and not an experimental artifact. Therefore, the observed solute rejections were converted to actual (or intrinsic) rejections to account for the local increase in the concentration of rejected solutes at the film interface due to concentration polarization.[35] The mass transfer coefficient necessary for this calculation was determined using the correlation

given by Zeman and Zydney.[36] For all rejection experiments, the ratio of the volumetric flux to the mass transfer coefficient was between 0.7 and 1.6, indicating that the system was not highly polarized.

Figure 2.5c shows the pore diameter of the films as calculated by comparing the actual rejection to a theory for the hindered transport of solutes in cylindrical pores. Because convection dominates transport through the mesopores, the theory of Zeman and Wales was used.[37]

$$R = 1 - \left[(1-\lambda)^2\left[2-(1-\lambda)^2\right]\exp\left(-0.7146\lambda^2\right)\right] \quad (1)$$

This simplified expression for the solute rejection, R, which gives results within 2% of more complicated expressions,[36] is a function of λ, defined as the ratio of the solute size to the pore size. The hydrodynamic radius of PEO, R_H, was taken as the characteristic solute size. R_H can be calculated from either tracer diffusion[38] or intrinsic viscosity[39] data sets, both of which are available in the literature. Using d_{pore} as an adjustable parameter, the residual squared was minimized. This method gave d_{pore} values of 15.9 and 21.8 nm when tracer diffusion and intrinsic viscosity were used to determine $2R_H$, respectively, and are in good agreement with the SEM micrograph in Figure 2.3.

The ability to finely tune structural parameters by hybridization with other materials, thus tailoring, e.g., the transport properties of the terpolymer films, is another exciting feature of these materials. For example, hybrid films fabricated by blending of a homopolymer that preferentially partitions into one domain of the block terpolymer can be utilized. These terpolymer-homopolymer blends selectively

increase the size of the specified terpolymer domain, as demonstrated by the results shown in Figure 2.5. Here, P4VP homopolymer with molar mass 5.1 kg/mol and polydispersity 1.06 was blended with the terpolymer in the casting solution to swell the effective volume fraction of P4VP from 0.15 to 0.22. Transport tests were used to confirm this observation. The open square data in Figure 2.5a shows that these hybrid films remain stimuli responsive. At pH = 4, the permeability is equal to 5.4 L $m^{-2}h^{-1}bar^{-1}$, which is about 50 times lower than the permeability at pH = 5.2 of 274 L $m^{-2}h^{-1}bar^{-1}$. These permeabilities measured for the hybrid ISV-77 films are higher than those of the neat ISV-77 films at the same pH, consistent with an increased pore size. Additionally, visual comparison of the pores in the top surface of parent ISV-77 films against homopolymer blended ISV-77 films, shown in Appendix A, Figure A.1, confirms that the homopolymer increases the pore diameter.

Figure 2.5b shows the results of solute rejection tests conducted with the hybrid membranes (square symbols). These experiments were run at a lower pressure drop to maintain similar hydrodynamic conditions to those used when testing the parent membrane. Following the protocol discussed above, an increased pore diameter of 21.3 and 29.7 nm was calculated for the hybrid membrane depending on whether tracer diffusion or intrinsic viscosity data was used to calculate the R_H of PEO. Figure 2.5c shows the fit obtained when intrinsic viscosity data was used to calculate the characteristic size of PEO.

A summary of the hydraulic permeabilities and estimated pore sizes for the parent and hybrid films is given as a table in Figure 2.5d. Interestingly, the ratio of the hydraulic permeabilities of the hybrid to the parent film is 1.78, while the ratio of the

product of the P4VP volume fraction and pore diameters squared is equal to 2.76 and 2.85 for tracer diffusion and intrinsic viscosity, respectively. Given that the hydraulic permeability of a membrane should vary as $\varepsilon \cdot d_{pore}^2$, where ε is the void fraction of pores,[40] the lack of a corresponding increase in the ratio for the hybrid membranes suggests an inhibition of flow due to the macroporous support structure. While the homopolymer appears to act as a pore-forming agent in the substructure, as seen from a comparison of the insets of Figure 2.2b and 2.2c, we expect that further improvements in the phase inverted structure would enhance the flux gain exhibited by the blended materials.

With the knowledge gained from the materials characterization and transport experiments, it is instructive to return to Figure 2.1a and consider the physical processes occurring as the kinetically-trapped mesostructure of the selective layer develops. When dissolved in the casting solution, the ISV self-assembles into micelles with PI cores and an outer P4VP corona, which minimizes the unfavorable enthalpic interactions between the casting solvents and the PI chains (see table in Figure 2.1). We speculate that as the solvent evaporates from the film/air interface, and the local concentration of polymer increases, the terpolymer micelles begin to pack cubically. With further solvent evaporation, the terpolymer eventually feels a driving force to transition to the equilibrium hexagonal cylinder morphology. It has been proposed that the solvent concentration gradient when the micelles begin to transition to a cylinder morphology is responsible for orienting the cylinders perpendicular to the thin dimension of the film.[29] Upon plunging the film into the non-solvent, the solvent and non-solvent begin to exchange, causing the ISV to precipitate, trapping the final

structure of the selective layer. We hypothesize that the exchange of solvent and non-solvent also results in the creation of free volume with the P4VP cylinders; as the solvent-swollen P4VP chains within the cylinders come into contact with the non-solvent, they collapse against the cylinder walls, forming channels of free volume within the cylinders, which is consistent with the observed stimuli responsive transport properties. The presence of free volume is also supported by the solute rejection curves in Figure 2.5b, which demonstrate a size exclusion rejection, consistent with open pores.

In summary, the results presented here demonstrate the benefits of moving from diblock copolymers to multiblock polymers and their hybrids for the formation of high performance graded mesoporous materials. Specifically, the tunable structural characteristics, adjustable mechanical properties, and controllable chemical functionalities of multiblock systems, provide an exceptional platform for the fabrication of graded mesoporous materials. Due to enhancements possible through terpolymers, detailed empirical studies of transport phenomena at the mesoscale were possible, and we anticipate that this study will expand the viability of such multiblock polymer-derived graded structures to a wide variety of fields.

Methods

The poly(isoprene-*b*-styrene-*b*-4-vinylpyridine) triblock terpolymer used in this study was synthesized using a sequential anionic polymerization technique. A detailed description of the synthesis can be found in Appendix A. The molecular weight of the terpolymer was determined using gel permeation chromatography, which was

performed using THF as a solvent on a Waters 510 GPC instrument equipped with a Waters 2410 differential refractive index (RI) detector. The volume fraction of each block was calculated using the ^1H solution nuclear magnetic resonance (^1H NMR) spectra obtained on a Varian INOVA 400 MHz spectrometer using $CDCl_3$ (δ = 7.27 ppm) signal as an internal standard.

Large sheets of mesoporous films were cast using the protocol described in the text. Circular samples 2.5 cm in diameter for solvent flow and solute rejection tests were punched out of larger sheets using a hole punch.

Solvent flow experiments were conducted in a stirred cell (Amicon 8010, Millipore Co.). Pressure to drive flow was applied using N_2 gas and was monitored using a digital pressure gauge. Deionized water (DI) was obtained from a Milli-Q ultrapure water purification system. Acetate buffer solutions were prepared by mixing 0.1 M acetic acid and 0.1 M sodium acetate aqueous solutions in the proper proportions. The flow rate was determined by measuring the permeate mass every 5 minutes. No prewetting step was required for the solvent flow experiments.

Solute rejection tests were performed using single solute PEO solutions at a concentration of 1 g/L in DI. The experimental procedure followed was similar to that described in the literature.[16] PEO concentration in the feed and permeate was determined using a Shimadzu total organic carbon analyzer. For all experiments, the solution was stirred at a rate of 800 rpm. Tests on the ISV-77 films were run at a constant pressure drop of 5 psi while tests on the swollen ISV-77 films were run at a pressure drop of 3 psi to maintain similar hydrodynamic conditions between the two samples.

For TEM, both the bulk polymer film and the membranes were sectioned at 50-70 nm using a Leica Ultracut UCT cryo-ultramicrotome at -60 °C. Microtomed samples were selectively stained with either OsO_4 (g) for 30 minutes or with I_2 (g) for 2 hours. Bright field TEM (BF-TEM) images were obtained using a FEI Technai F12 Spirit electron microscope equipped with a SIS Megaview III CCD camera, operated at an acceleration voltage of 120 kV.

SEM micrographs were acquired using a Hitachi Ultra-High Resolution Analytical Field Emission Scanning Electron Microscope (FE-SEM) SU-70. Samples were coated with gold-platinum for 30 s prior to imaging using an Emitech SC7620 sputtering machine.

SAXS measurements on the bulk terpolymer were performed at the Cornell High Energy Synchrotron Source (CHESS). The sample to detector distance was approximately 3.3 m. The x-ray wavelength was 1.305 Å, and the scattering vector, q, is defined as $q = \frac{4\pi}{\lambda}\sin\theta$ where θ is half of the scattering vector.

Mechanical tests were performed using a TA Instruments DMAQ800 instrument outfitted with film tension clamps. The films were fixed in the tension clamps with a torque of 0.6 in lb. and preloaded with a force of 0.01 N. Stress-strain curves were obtained using a ramp force of 0.50 N/min.

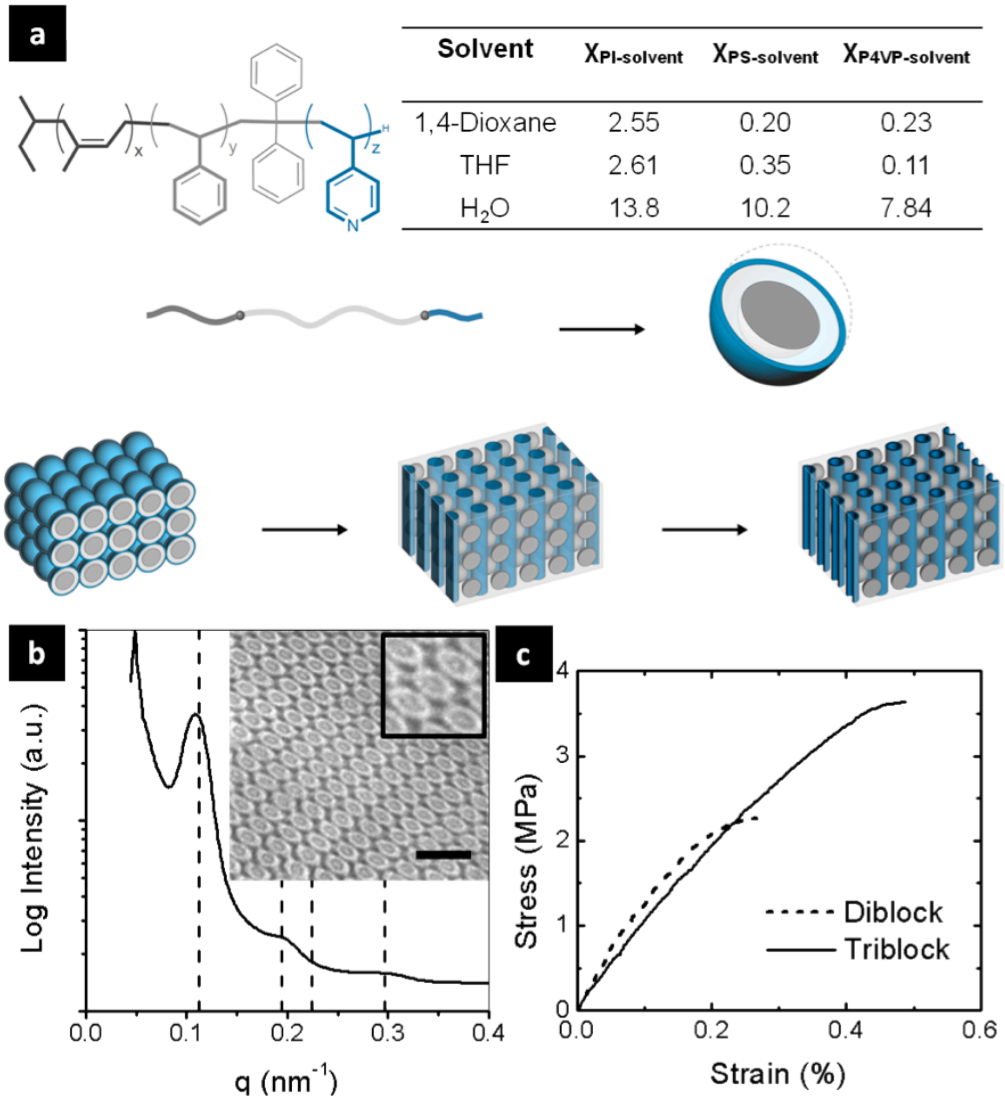

Figure 2.1 Mesoporous films are cast from a poly(isoprene-*b*-styrene-*b*-4-vinyl pyridine) triblock terpolymer. a. The structure of the ISV terpolymer, table indicating the polymer-solvent interaction parameters as calculated from solubility parameters, and proposed formation mechanism of the separation layer. **b.** Small-angle X-ray scattering (SAXS) trace of the bulk ISV material. Dashed lines correspond to peak positions $(q/q^*)^2$ = 1, 3, 4, and 7, expected for a hexagonal lattice. Inset: TEM image of the terpolymer film selectively stained with OsO_4. The scale bar is 100 nm.

The higher magnification inset displays the interconnected white polystyrene regions and is 100 nm on each side. The darkest regions correspond to the PI, the gray regions to the P4VP, and the white regions to the PS domains. **c.** Stress-strain curves of the bulk triblock terpolymer and diblock copolymer films.

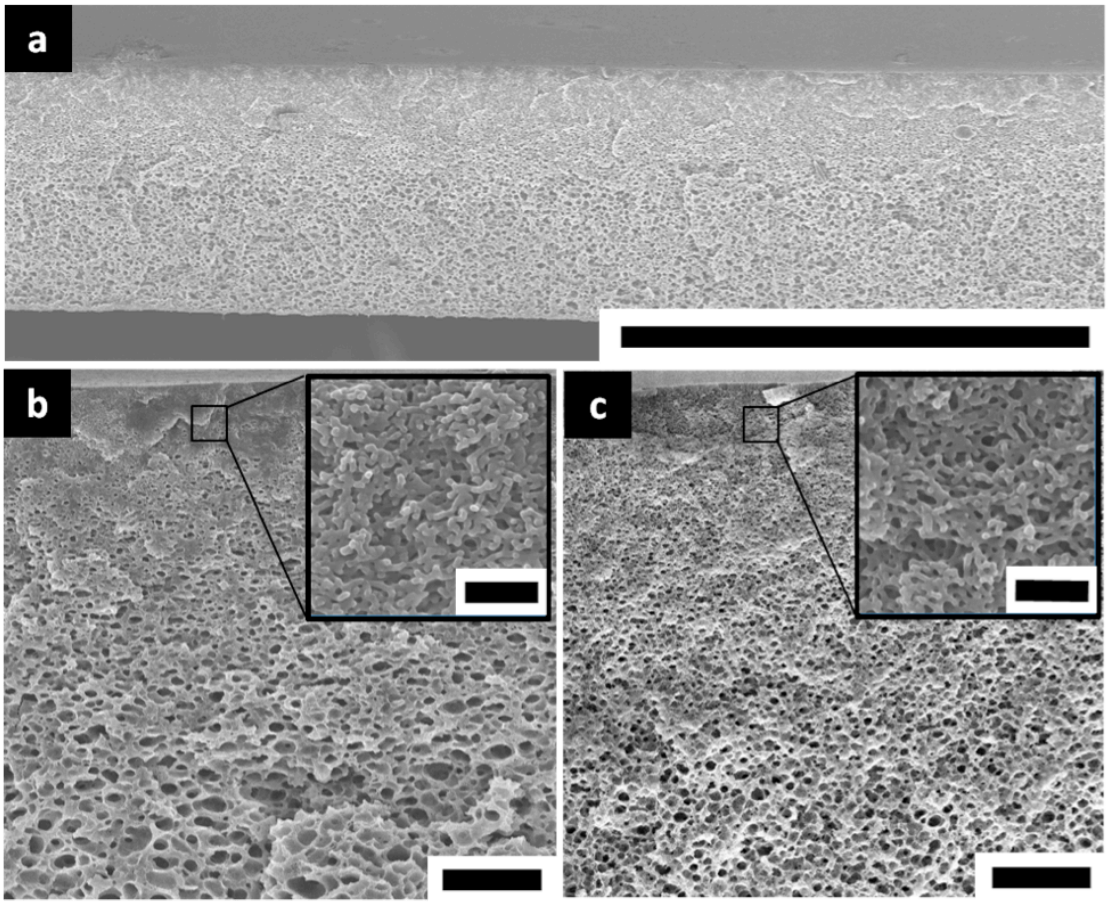

Figure 2.2 The non-solvent induced phase separation process forms a sponge-like, graded structure in the membranes. **a.** Low-magnification SEM micrograph of the cross-section of an ISV-77 film. Scale bar is 100 μm **b.** Cross-sectional SEM of the as cast parent terpolymer film shows that the bottom of the film is macroporous and becomes denser as proximity to the top selective layer increases. Inset: higher magnification image of the phase inverted structure just below the separation layer shows that the region contains macropores. **c.** Cross-sectional SEM of the hybrid membrane displaying a similar graded structure. Inset: higher magnification image of the phase inverted structure just below the separation layer displays increased porosity compared to the parent structure. The scale bars for panels b and c are 5 μm and 500

nm in the main images and insets, respectively.

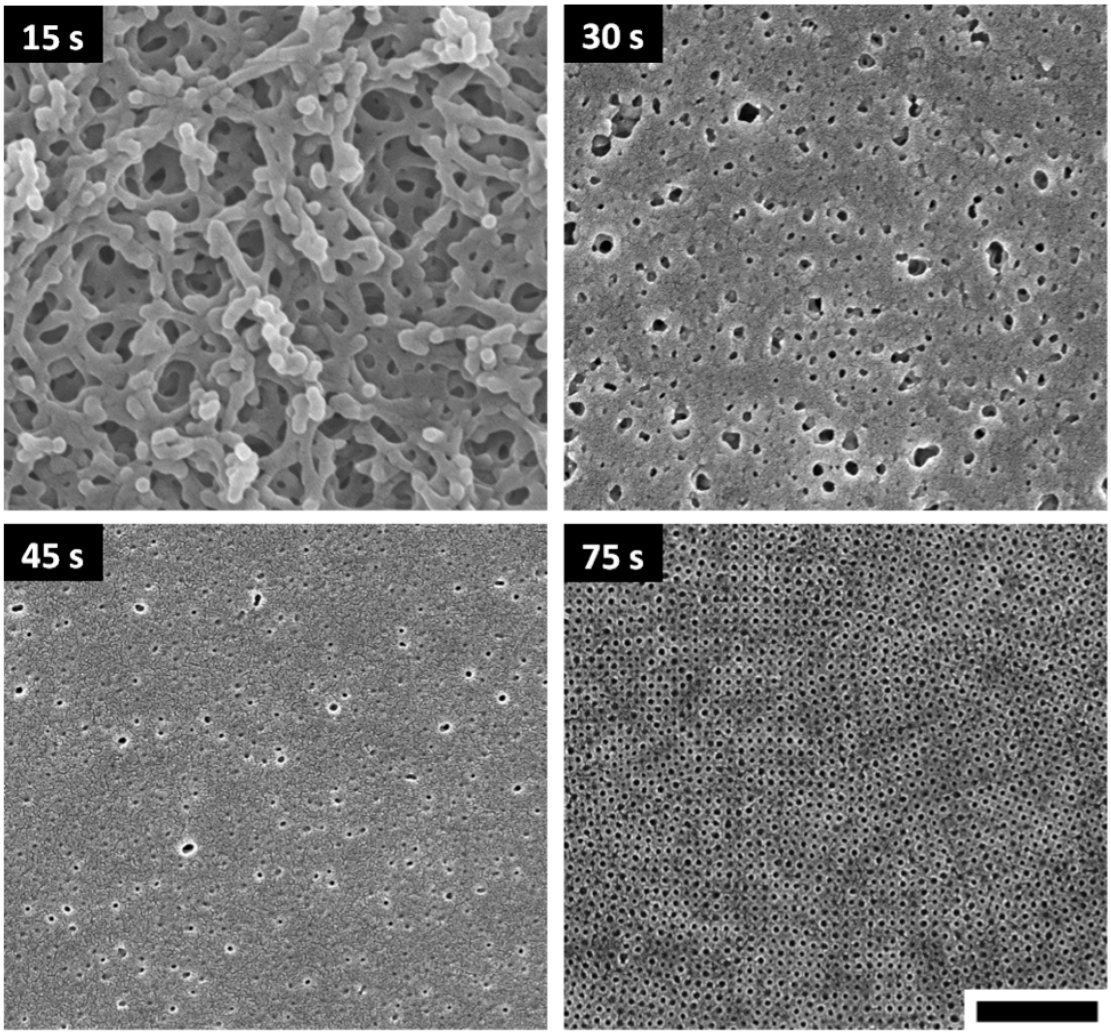

Figure 2.3 SEM micrographs show that the structure of the thin film surface changes with the length of the solvent evaporation period. Poly(isoprene-*b*-styrene-*b*-4 vinyl pyridine) thin films were cast from a 12 wt% solution of polymer in solvent. The solvent used was a 70/30 mixture (w/w) of dioxane and tetrahydrofuran (THF). After drawing down a thin film of polymer solution, solvent was allowed to evaporate for a predetermined period of time before plunging the film into a non-solvent (water) bath to initiate phase separation. For short evaporation times (15 and 30 seconds), a dense layer does not form, producing macroporous films. At

intermediate evaporation times (45 seconds) a dense layer forms, but the self-assembled terpolymer structure has just begun to nucleate resulting in few pores. Given sufficient time (75 seconds), the self-assembled structure nucleates and grows into the film producing a thin film with a high density of nanopores. All images are shown at the same resolution and the scale bar is 500 nm.

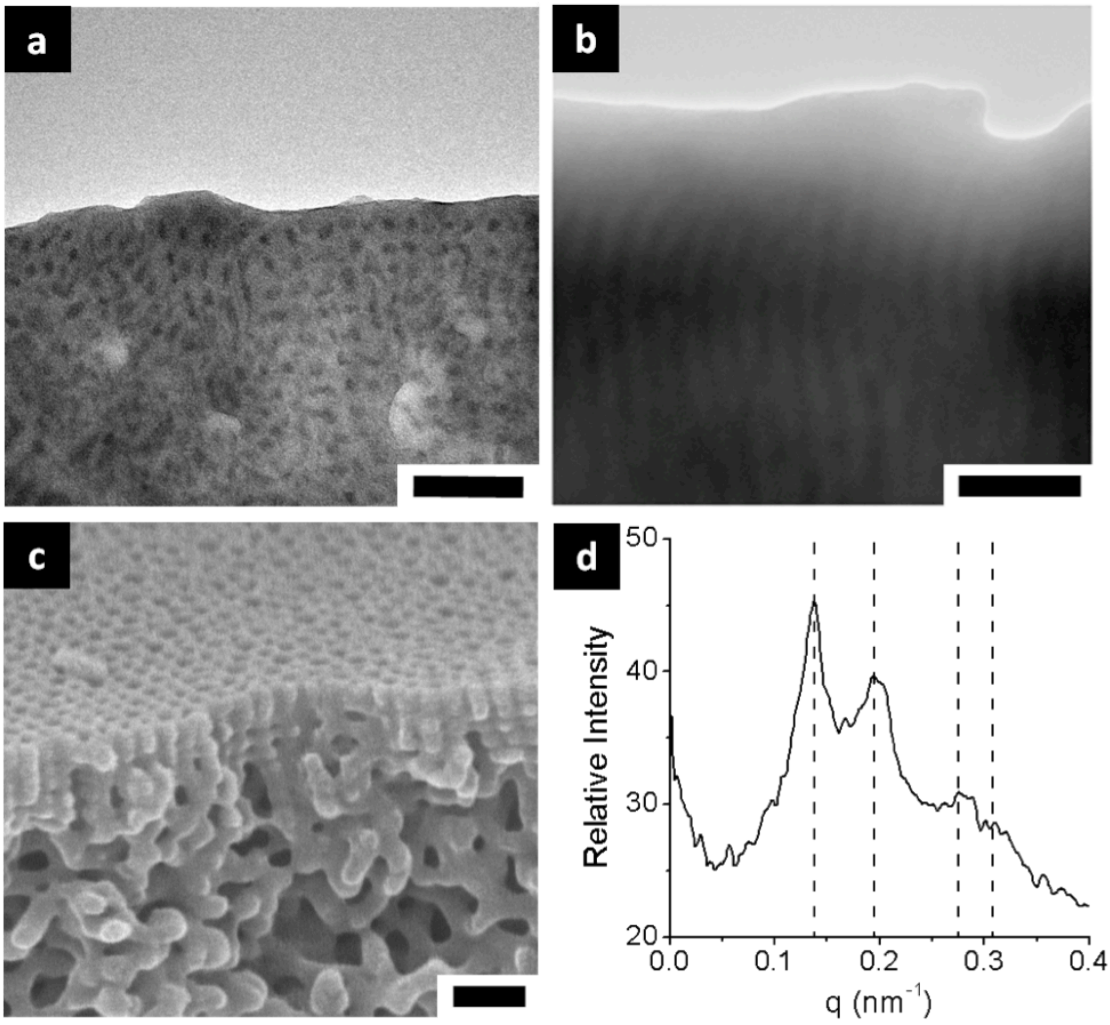

Figure 2.4 The self-assembled structure of the selective layer is a kinetically trapped, non-equilibrium structure. a. Cubically packed polyisoprene spheres are identified by TEM where the PI domains were stained with OsO_4. **b.** A TEM micrograph of the selective layer with P4VP domains stained with I_2 demonstrates P4VP channels run through the selective layer. **c.** A cross sectional SEM micrograph shows open pores spanning the selective layer thickness, consistent with the I_2 stained TEM micrograph. All scale bars are equal to 100 nm. **d.** Radially integrated FFT of an SEM image of the top surface of the film. Dashed lines correspond to $(q/q^*)^2 = 1, 2, 4,$

and 5, consistent with pores packed in a square lattice and yielding a d-spacing of 44 nm.

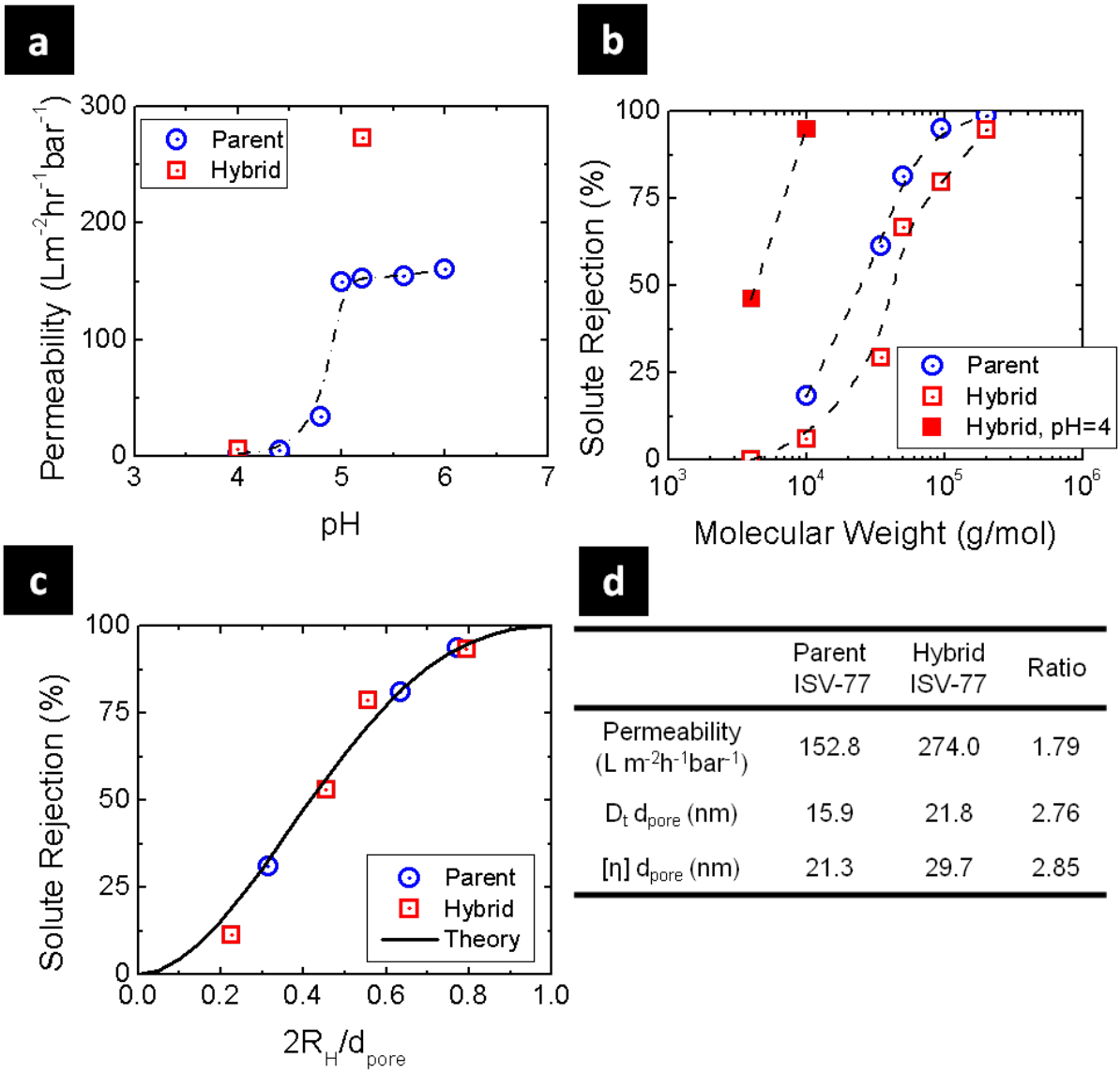

d

	Parent ISV-77	Hybrid ISV-77	Ratio
Permeability ($L\ m^{-2}h^{-1}bar^{-1}$)	152.8	274.0	1.79
D_t d_{pore} (nm)	15.9	21.8	2.76
[η] d_{pore} (nm)	21.3	29.7	2.85

Figure 2.5 Transport behavior of the mesoporous parent and hybrid films. a. Solution permeation was measured on a 4.1 cm^2 area of membrane at a pressure drop of 0.345 bar using buffer solutions of sodium acetate and acetic acid at varying pH. For membranes cast without swelling agents the hydraulic permeability ranges from 2.2 L $m^{-2}h^{-1}bar^{-1}$ to 160 L $m^{-2}h^{-1}bar^{-1}$ at pH = 4 to pH = 6, respectively. Membranes cast with swelling agents had a hydraulic permeability of 5.4 L $m^{-2}h^{-1}bar^{-1}$ at pH = 4 and 274 L $m^{-2}h^{-1}bar^{-1}$ at pH = 5.2. **b.** The nanoporous thin films reject dissolved

solutes. Polyethylene oxide molecules with molar masses of 4, 10, 35, 50, 95, and 203 kg/mol were dissolved in water at a concentration of 1 g/L. Feed and permeate samples were collected and the PEO concentrations determined using total organic carbon analysis. **c.** The pore size of the ISV-77 and hybrid ISV-77 films are estimated by fitting the experimental rejection data with a theory for the hindered transport of solutes in cylindrical pores. The data point at $2R_H/d_{pore} \approx 0.8$ for the parent ISV-77 film is for the 50 kg/mol PEO molecule while for the hybrid ISV-77 film it is for the 95 kg/mol PEO sample. **d.** Table of the hydraulic permeabilites and calculated pore diameters from diffusion and intrinsic viscosity data. For the hydraulic permeabilities, the ratio column is the quotient of the two values, while for the pore diameter this column represents the ratio of $\varepsilon \cdot d_{pore}^2$.

REFERENCES

1. Shannon, M. A.; Bohn, P. W.; Elimelech, M.; Georgiadis, J. G.; Marinas, B. J.; Mayes, A. M., Science and technology for water purification in the coming decades. *Nature* **2008,** *452* (7185), 301-310.

2. van Reis, R.; Zydney, A., Bioprocess membrane technology. *Journal of Membrane Science* **2007,** *297* (1-2), 16-50.

3. Bohn, P. W., Nanoscale Control and Manipulation of Molecular Transport in Chemical Analysis. *Annual Review of Analytical Chemistry* **2009,** *2* (1), 279-296.

4. Jackson, E. A.; Hillmyer, M. A., Nanoporous Membranes Derived from Block Copolymers: From Drug Delivery to Water Filtration. *Acs Nano* **2010,** *4* (7), 3548-3553.

5. Hillmyer, M., Nanoporous Materials from Block Copolymer Precursors. In *Block Copolymers II*, Abetz, V., Ed. Springer Berlin / Heidelberg: 2005; Vol. 190, pp 137-181.

6. Park, M.; Harrison, C.; Chaikin, P. M.; Register, R. A.; Adamson, D. H., Block copolymer lithography: Periodic arrays of similar to 10(11) holes in 1 square centimeter. *Science* **1997,** *276* (5317), 1401-1404.

7. Kim, S. O.; Solak, H. H.; Stoykovich, M. P.; Ferrier, N. J.; de Pablo, J. J.; Nealey, P. F., Epitaxial self-assembly of block copolymers on lithographically defined nanopatterned substrates. *Nature* **2003,** *424* (6947), 411-414.

8. Singh, M.; Odusanya, O.; Wilmes, G. M.; Eitouni, H. B.; Gomez, E. D.; Patel, A. J.; Chen, V. L.; Park, M. J.; Fragouli, P.; Iatrou, H.; Hadjichristidis, N.; Cookson,

D.; Balsara, N. P., Effect of molecular weight on the mechanical and electrical properties of block copolymer electrolytes. *Macromolecules* **2007,** *40* (13), 4578-4585.

9. Panday, A.; Mullin, S.; Gomez, E. D.; Wanakule, N.; Chen, V. L.; Hexemer, A.; Pople, J.; Balsara, N. P., Effect of Molecular Weight and Salt Concentration on Conductivity of Block Copolymer Electrolytes. *Macromolecules* **2009,** *42* (13), 4632-4637.

10. Crossland, E. J. W.; Kamperman, M.; Nedelcu, M.; Ducati, C.; Wiesner, U.; Smilgies, D. M.; Toombes, G. E. S.; Hillmyer, M. A.; Ludwigs, S.; Steiner, U.; Snaith, H. J., A Bicontinuous Double Gyroid Hybrid Solar Cell. *Nano Letters* **2009,** *9* (8), 2807-2812.

11. Segalman, R. A.; McCulloch, B.; Kirmayer, S.; Urban, J. J., Block Copolymers for Organic Optoelectronics. *Macromolecules* **2009,** *42* (23), 9205-9216.

12. Orilall, M. C.; Matsumoto, F.; Zhou, Q.; Sai, H.; Abruna, H. D.; DiSalvo, F. J.; Wiesner, U., One-Pot Synthesis of Platinum-Based Nanoparticles Incorporated into Mesoporous Niobium Oxide-Carbon Composites for Fuel Cell Electrodes. *Journal of the American Chemical Society* **2009,** *131* (26), 9389-9395.

13. Cooney, D. L., Hillmyer, M. A., Cussler, E. L., Moggridge, G. D., Diffusion In Nanoporous Materials Made from Block Copolymers. *Crystallography Reviews* **2006,** *12* (1), 13-24.

14. Phillip, W. A.; Rzayev, J.; Hillmyer, M. A.; Cussler, E. L., Gas and water liquid transport through nanoporous block copolymer membranes. *Journal of Membrane Science* **2006,** *286* (1-2), 144-152.

15. Phillip, W. A.; Amendt, M.; O'Neill, B.; Chen, L.; Hillmyer, M. A.; Cussler, E. L., Diffusion and Flow Across Nanoporous Polydicyclopentadiene-Based Membranes. *Acs Applied Materials & Interfaces* **2009,** *1* (2), 472-480.

16. Phillip, W. A.; O'Neill, B.; Rodwogin, M.; Hillmyer, M. A.; Cussler, E. L., Self-Assembled Block Copolymer Thin Films as Water Filtration Membranes. *Acs Applied Materials & Interfaces* **2010,** *2* (3), 847-853.

17. Yang, S. Y.; Ryu, I.; Kim, H. Y.; Kim, J. K.; Jang, S. K.; Russell, T. P., Nanoporous membranes with ultrahigh selectivity and flux for the filtration of viruses. *Advanced Materials* **2006,** *18* (6), 709-+.

18. Li, X. F.; Fustin, C. A.; Lefevre, N.; Gohy, J. F.; De Feyter, S.; De Baerdemaeker, J.; Egger, W.; Vankelecom, I. F. J., Ordered nanoporous membranes based on diblock copolymers with high chemical stability and tunable separation properties. *Journal of Materials Chemistry* **2010,** *20* (21), 4333-4339.

19. Yang, S. Y.; Park, J.; Yoon, J.; Ree, M.; Jang, S. K.; Kim, J. K., Virus filtration membranes prepared from nanoporous block copolymers with good dimensional stability under high pressures and excellent solvent resistance. *Advanced Functional Materials* **2008,** *18* (9), 1371-1377.

20. Kim, J. K.; Yang, S. Y.; Yang, J. A.; Kim, E. S.; Jeon, G.; Oh, E. J.; Choi, K. Y.; Hahn, S. K., Single-File Diffusion of Protein Drugs through Cylindrical Nanochannels. *Acs Nano* **2010,** *4* (7), 3817-3822.

21. Peinemann, K. V.; Abetz, V.; Simon, P. F. W., Asymmetric superstructure formed in a block copolymer via phase separation. *Nature Materials* **2007,** *6* (12), 992-996.

22. Nunes, S. P.; Sougrat, R.; Hooghan, B.; Anjum, D. H.; Behzad, A. R.; Zhao, L.; Pradeep, N.; Pinnau, I.; Vainio, U.; Peinemann, K. V., Ultraporous Films with Uniform Nanochannels by Block Copolymer Micelles Assembly. *Macromolecules* **2010,** *43* (19), 8079-8085.

23. Hansen, C. M., *Hansen Solubility Parameters: A User's Handbook*. CRC Press: Boca Raton, FL, 2000.

24. Young, R. J., Lovell, P. A. , *Introduction to Polymers*. 2 ed.; CRC Press: Boca Raton, FL, 1991.

25. Phatak, A.; Lim, L. S.; Reaves, C. K.; Bates, F. S., Toughness of glassy-semicrystalline multiblock copolymers. *Macromolecules* **2006,** *39* (18), 6221-6228.

26. Alward, D. B.; Kinning, D. J.; Thomas, E. L.; Fetters, L. J., Effect of Arm Number and Arm Molecular-Weight on the Solid-State Morphology of Poly(Styrene-Isoprene) Star Block Copolymers. *Macromolecules* **1986,** *19* (1), 215-224.

27. Dair, B. J.; Honeker, C. C.; Alward, D. B.; Avgeropoulos, A.; Hadjichristidis, N.; Fetters, L. J.; Capel, M.; Thomas, E. L., Mechanical properties and deformation behavior of the double gyroid phase in unoriented thermoplastic elastomers. *Macromolecules* **1999,** *32* (24), 8145-8152.

28. Mulder, M., *Basic Principles of Membrane Technology*. 2nd ed.; Springer: 1996; p 564.

29. Phillip, W. A.; Hillmyer, M. A.; Cussler, E. L., Cylinder Orientation Mechanism in Block Copolymer Thin Films Upon Solvent Evaporation. *Macromolecules* **2010,** *43* (18), 7763-7770.

30. Baker, R. W., *Membrane technology and applications*. McGraw-Hill: New

York, 2000; p xii, 514 p.

31. Kim, G.; Libera, M., Morphological development in solvent-cast polystyrene-polybutadiene-polystyrene (SBS) triblock copolymer thin films. *Macromolecules* **1998,** *31* (8), 2569-2577.

32. Donald, A. M.; Kramer, E. J., Craze Initiation and Growth in High-Impact Polystyrene. *Journal of Applied Polymer Science* **1982,** *27* (10), 3729-3741.

33. Mika, A. M.; Childs, R. F.; Dickson, J. M., Chemical valves based on poly(4-vinylpyridine)-filled microporous membranes. *Journal of Membrane Science* **1999,** *153* (1), 45-56.

34. Tagliazucchi, M.; Azzaroni, O.; Szleifer, I., Responsive Polymers End-Tethered in Solid-State Nanochannels: When Nanoconfinement Really Matters. *Journal of the American Chemical Society* **2010,** *132* (35), 12404-12411.

35. Mehta, A.; Zydney, A. L., Permeability and selectivity analysis for ultrafiltration membranes. *Journal of Membrane Science* **2005,** *249* (1-2), 245-249.

36. Zeman, L. J.; Zydney, A. L., *Microfiltration and ultrafiltration : principles and applications*. M. Dekker: New York, 1996; p xix, 618 p.

37. Zeman, L.; Wales, M., Polymer Solute Rejection by Ultrafiltration Membranes. In *Synthetic Membranes: Volume II*, AMERICAN CHEMICAL SOCIETY: 1981; Vol. 154, pp 411-434.

38. Faraone, A.; Magazu, S.; Maisano, G.; Migliardo, P.; Tettamanti, E.; Villari, V., The puzzle of poly(ethylene oxide) aggregation in water: Experimental findings. *Journal of Chemical Physics* **1999,** *110* (3), 1801-1806.

39. Meireles, M.; Bessieres, A.; Rogissart, I.; Aimar, P.; Sanchez, V., An

Appropriate Molecular-Size Parameter for Porous Membranes Calibration. *Journal of Membrane Science* **1995,** *103* (1-2), 105-115.

40. Bird, R. B.; Stewart, W. E.; Lightfoot, E. N., *Transport phenomena*. 2nd ed.; John Wiley & Sons, Inc.: New York ; Chichester, 2002; p xii, 895 p.

CHAPTER 3

Solution Small-Angle X-ray Scattering as a Screening and Predictive Tool in the Fabrication of Asymmetric Block Copolymer Membranes*

Abstract

Optimizing casting solution formulations in the preparation of block copolymer asymmetric membranes remains a tedious and inefficient trial and error process. Small-angle x-ray scattering (SAXS) analysis of the diblock copolymer poly(styrene-*b*-(4-vinyl)pyridine) (SV) in a ternary solvent system of 1,4-dioxane, tetrahydrofuran, and N,N-dimethylforamide, and the triblock terpolyer poly(isoprene-*b*-styrene-*b*-(4-vinyl)pyridine) (ISV) in a binary solvent system of 1,4-dioxane and tetrahydrofuran, reveals a concentration dependent onset of ordered structure formation. Asymmetric membranes fabricated from casting solutions with polymer concentrations below this ordering concentration possess selective layers with the desired nanostructure. In addition to rapidly screening possible polymer solution concentrations, solution SAXS analysis also predicts hexagonal and square pore lattices of the final membrane surface structure. These results demonstrate solution SAXS as a powerful tool for screening casting solution concentrations and predicting surface structure in the fabrication of asymmetric ultrafiltration membranes from self-assembled block copolymers.

* Reproduced with permission from Dorin, R. M.; Marques, D. S.; Sai, H.; Vainio, U.; Phillip, W. A.; Peinemann, K.-V.; Nunes, S. P.; Wiesner, U., Solution Small-Angle X-ray Scattering as a Screening and Predictive Tool in the Fabrication of Asymmetric Block Copolymer Membranes. *ACS Macro Letters* **2012,** *1* (5), 614-617. Copyright 2012 American Chemical Society.

A critical challenge in producing high performance membranes from block copolymers is understanding and controlling the solution behavior of these unique, self-assembling materials.[1-5] Insight into this behavior will enable the application of block copolymers in membrane technologies, including water purification,[6] drug delivery,[7] and bioprocessing,[8] as well as in photovoltaic[9] and battery[10] technologies. Previously, membranes have been fabricated from block copolymers using spin-coating,[7,11-13] extrusion,[14,15] and bulk evaporation[6,16,17] techniques, yet the membranes produced from these methods typically require post-fabrication modifications to convey porosity onto the films and are not based on proven industrial processes. Recently, the self-assembling nature of block copolymers has been exploited for the production of high performance isoporous membranes from both diblock copolymers[3,5,18,19] and triblock terpolymers[4] using a combined Self-assembly and Non-Solvent Induced Phased Separation, or SNIPS, method. This method does not require post-fabrication modifications and is based on the industry standard phase separation technique. The SNIPS method involves dissolving the block copolymer in a solvent or mixed-solvent system to produce a casting solution, which is doctor-bladed into a film, solvent is then evaporated for a period of tens of seconds before immersing the film into a coagulation bath. The process results in membranes with a high density of uniform pores (typically $>10^{14}$ pores/cm2) in the top separation layer above a macroporous, asymmetric substructure. The structural characteristics of membranes formed using the SNIPS method directly enhance membrane performance; uniform pore sizes in the selective layer result in efficient separations while high pore densities

yield high fluxes. Furthermore, the asymmetric substructure provides mechanical support for the selective layer.

The functionality of the SNIPS process has been demonstrated by the successful production of diblock copolymer and triblock terpolymer membranes. However, determining the composition of the block copolymer casting solution, in particular when new polymer systems are investigated, remains a major challenge. The casting solvents or solvent mixtures and the block copolymer concentrations are dictated by a complex set of thermodynamic and kinetic factors, and system optimization is a tedious and inefficient trial and error process. An additional challenge is the apparent small phase window over which the desired membrane structure can be achieved. Rapid expansion of the SNIPS method to new polymer systems therefore necessitates an efficient screening tool that allows for the quick and easy evaluation of casting solutions. Recent work has shown that the structure of the casting solution significantly affects the final structure of a block copolymer membrane produced using the SNIPS process[3]. In order to quantitatively investigate the long-range nanoscale structure in the polymer casting solutions, we investigated the following two systems: diblock copolymer poly(styrene-*b*-(4-vinyl)pyridine) with a total molecular weight of 240 kg/mol (SV-240) in a ternary solvent mixture of 1,4-dioxane (DOX), tetrahydrofuran (THF), and N,N-dimethylforamide (DMF), and the triblock terpolymer poly(isoprene-*b*-styrene-*b*-(4-vinyl)pyridine) with a total molecular weight of 59 kg/mol (ISV-59) in a binary solvent mixture of DOX and THF. Both systems were evaluated at different concentrations using small angle x-ray scattering (SAXS).

The ratio of solvents for each system was kept constant with a DOX:THF:DMF ratio of 1:1:1 by weight for SV-240 and with a DOX:THF ratio of 7:3 by weight for ISV-59. The series of SAXS patterns for SV-240, shown in Figure 3.1a, indicates that the copolymer solution developed from a disordered structure with only a broad correlation peak at lower concentrations (e.g. 14 and 15 wt %), into a structured solution exhibiting a pattern consistent with a 2D hexagonal structure at 17 wt% (see also Appendix B, Figure B.1 for SAXS at 22% corroborating this assignment). Analysis of the SAXS pattern for the structured solution suggests a lattice constant of 88.0 nm. A similar behavior was observed in the ISV-59 concentration series. At lower polymer concentrations (see 10, 12 and 14 wt% solution data in Figure 3.1b) only a broad correlation peak was observed, suggesting a lack of long-range order in the solution. However, as the concentration increased to 16 wt%, the SAXS pattern changed and showed a set of peaks consistent with a body-centered cubic lattice. The corresponding lattice constant for the triblock system was 37.0 nm.

Membranes cast from solutions close to the onset concentrations for ordered solution structures resulted in well-organized asymmetric membranes. The full characterizations of such membranes for the diblock as well as the triblock copolymer are discussed in previous publications,[2,3] here we will only display and analyze representative SEM micrographs of the membrane surface. The active layer surfaces of membranes cast from 15 wt% SV-240 and 16 wt% ISV-59 using the SNIPS method are shown in Figures 3.2a and 3.2b, respectively. Both display uniform pore sizes and high pore densities. Visual inspection of the SEM micrographs in Figure 3.2a and 3.2b suggests that the top surface of the diblock membrane orders into a 2D hexagonal

structure while the top surface of the triblock membrane orders into a square lattice. Furthermore, both the pore size and spacing in the diblock appear significantly larger than that of the triblock, as expected from the difference in the polymer molar mass. Both the diblock and triblock solutions at the casting concentrations in their respective solvent systems were viscous and required care to minimize the inclusion of air bubbles. The onset concentration determined by solution SAXS is therefore an upper limit to the copolymer concentration as higher viscosity solutions would be difficult to doctor blade.

FFT analysis on the SEM micrograph followed by radial integration allowed a more quantitative evaluation of the membrane surface structure to be performed. The results from this analysis are displayed in Figure 3.3a and 3.3b for the diblock and triblock membranes, respectively. The dash markings in Figure 3.2a correspond to a 2D hexagonal pore packing in the separation layer of the diblock membrane, while the dashed markings in Figure 3.2b correspond to a 2D square lattice pore packing in the separation layer of the triblock membrane. The FFT analysis of the SV-240 membrane suggests a lattice constant of 92.0 nm, yielding a pore density of 1.36×10^{14} pores/m^2. The square lattice observed for the triblock membrane has a lattice constant of 34.3 nm, yielding a pore density of 8.20×10^{14} pores/m^2. Interestingly, the lattice dimensions of the final membranes closely match the lattice constants determined from solution SAXS of the casting solutions, suggesting that x-ray can also be used as a predictive tool for membrane pore density.

The fabrication of block copolymer membranes with a variety of chemical, mechanical, and structural properties could significantly advance the field of

membrane science. Having a powerful tool that enables more rapid screening of optimal solution concentrations and predicting surface structure may make fabrication of asymmetric ultrafiltration membranes, in particular from untested block copolymer systems, a more manageable task and may lead to a much faster expansion of this emerging research area.

Experimental Section

Materials. The diblock copolymer used in this study was purchased from Polymer Source, Inc., Canada and had a total molecular weight of 240 kg/mol, a polydispersity of 1.09, and volume fractions of 0.76 and 0.24 for polystyrene and poly-(4-vinyl)pyridine, respectively. The triblock terpolymer used in this study was synthesized via sequential anionic polymerization as previously reported.[4] It had a total molecular weight of 59 kg/mol, a polydispersity of 1.14 and volume fractions of 0.27, 0.55, and 0.18 for the polyisoprene, polystyrene, and poly-(4-vinyl)pyridine components, respectively. Tetrahydrofuran (THF), 1,4-dioxane (DOX), and N,N-dimethylforamide (DMF) were purchased from Aldrich and used as received.

Polymer Analysis. The molecular weight characteristics of the triblock terpolymer were determined by gel permeation chromatography, which was performed using THF as a solvent on a Waters 510 GPC instrument equipped with a Waters 2410 differential refractive index (RI) detector. The volume fraction of each block was calculated from ^{1}H solution nuclear magnetic resonance (^{1}H NMR) spectra obtained on a Varian INOVA 400 MHz spectrometer using $CDCl_3$ (δ = 7.27 ppm) signal as an internal standard.

SEM analysis. SEM micrographs of the diblock membrane were attained on an FEI Nova Nano 630. SEM micrographs of the tribock membranes were acquired using a Hitachi Ultra-High Resolution Analytical Field Emission Scanning Electron Microscope SEM SU-70.

Membrane formation. Diblock copolymer membranes were fabricated from a 15 wt% polystyrene-b-(4-vinyl)pyridine in 1:1:1 DOX:THF:DMF (by weight) and doctor blading at a gate height of 200 μm. The triblock terpolymer membranes were fabricated from a 16 wt % poly(isoprene-b-styrene-b-(4-vinyl)pyridine) in 7:3 DOX:THF (by weight) and doctor-blading at a gate height of 200 μm. The diblock film was evaporated for 20 seconds while the triblock film was evaporated for 30 seconds before immersion into a coagulation bath of deionized water.

SAXS solutions. Block copolymer solutions for SAXS measurements were prepared by dissolving the polymer at the specified concentrations in solvent mixtures at constant ratios of 1:1:1 DOX:THF:DMF by weight for the diblock and ratios of 7:3 DOX:THF by weight for the triblock. Solutions were injected via syringe into 2 mm and 1 mm capillaries for the diblock copolymer and triblock terpolymer, respectively. The capillaries were sealed using Hardman Fast 5 Minute epoxy.

SAXS measurements. SAXS measurements on the diblock copolymer solutions were performed at the beamline B1 at DORIS III synchrotron storage ring at the *Deutsches-Elektronen Synchrotron* (DESY) with a photon flux of $\sim 10^8$ photons/s while those on the triblock terpolymer solutions were measured at the beamline G1 at the Cornell High Energy Synchrotron Source (CHESS) with a photon flux of $\sim 10^{12}$ photons/s. The sample-to-detector distance was approximately 3.6 m at B1 and 3.3 m

at G1, and the x-ray wavelength, λ, was 1.764 and 1.305 Å, respectively. The scattering vector, q, is defined as $q = \frac{4\pi}{\lambda}\sin\theta$ where θ is half of the scattering angle.

SEM Image Analysis. FFT analysis was performed using ImageJ64 software on SEM images displaying the top surface of diblock and triblock copolymer membranes.

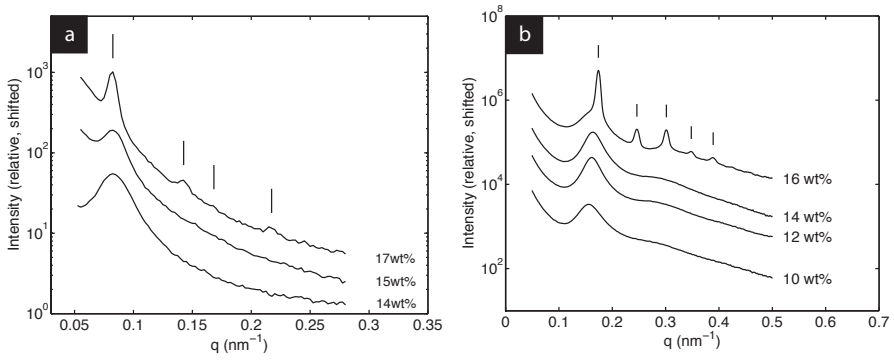

Figure 3.1 Small-angle X-ray scattering curves for SV-240 (a) and ISV-59 (b) at varying polymer concentrations in 1:1:1 DOX:THF:DMF by weight and 7:3 DOX:THF by weight, respectively. Dash markings in (a) correspond to expected peak positions for a 2D hexagonal lattice with a lattice constant of 88.0 nm, while dashed markings in (b) correspond to expected peak positions for a BCC lattice with a lattice constant of 37.0 nm.

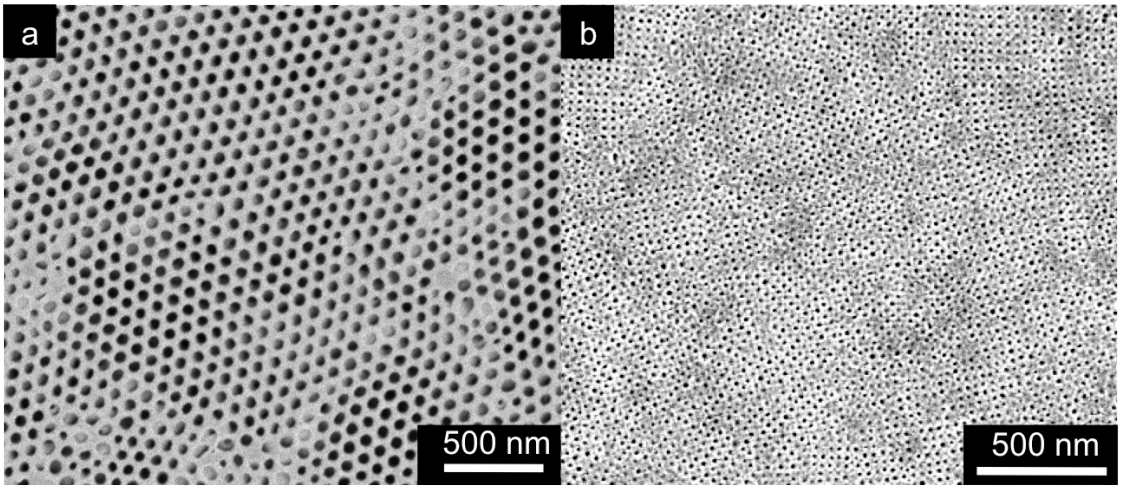

Figure 3.2 SEM characterization of block copolymer membrane structure. Self-assembled top surface of the diblock poly(styrene-b-(4-vinyl)pyridine) cast from DOX:THF:DMF 1:1:1 by weight from a 15 wt% solution (a) and of the triblock poly(isoprene-b-styrene-b-(4-vinyl)pyridine) in DOX:THF 7:3 by weight from a 16 wt% solution (b).

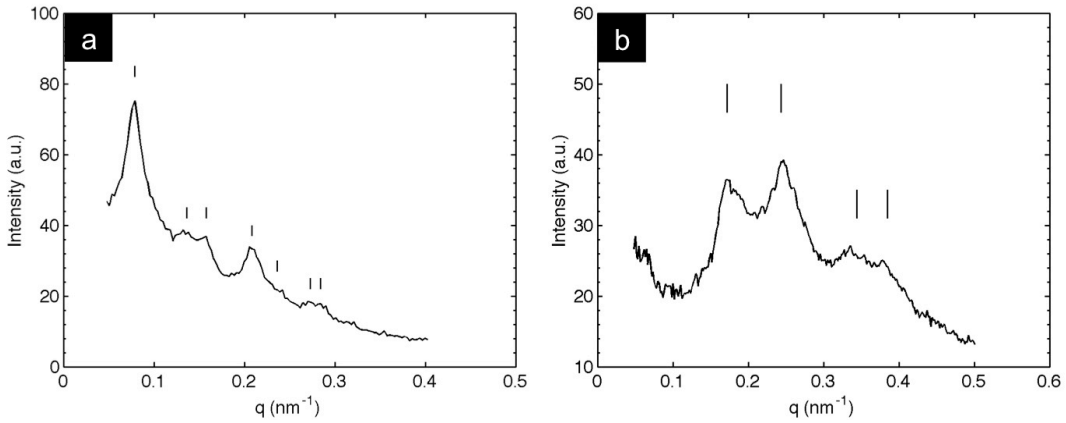

Figure 3.3 FFT Analysis of SEM images of the top surface diblock (a) and triblock (b) membranes. Dash markings in (a) correspond to $(q/q^*)^2$=1, 3, 4, 7, 9, 12, and 13, consistent with a 2D hexagonal structure, while dashed markings in (b) correspond to $(q/q^*)^2$=1, 2, 4, and 5, consistent with a 2D square lattice.

Acknowledgements

This work was funded in part by Award No. KUS-C1-018-02, made by King Abdullah University of Science and Technology (KAUST), a Partnership for Research and Education in materials (PREM) program at Norfolk State University through the National Science Foundation (NSF) grant (DMR-0611430 and DMR-1120296), and by the U.S. Department of Homeland Security under Cooperative Agreement Number "2009-ST-108-LR0004". Portions of this research were carried out at the light source DORIS III at DESY, a member of the Helmholtz Association (HGF). CHESS is supported by the NSF & NIH/NIGMS via NSF award DMR-0936384. This work was further supported by the National Science Foundation through a single investigator award (DMR-1104773). This work made use of the KAUST Core Lab and the Integrated Advanced Microscopy Facilities and Polymer Characterization Facility of the Cornell Center for Materials Research (CCMR) with support from the National Science Foundation Materials Research Science and Engineering Centers (MRSEC) program (DMR 1120296). R.M.D acknowledges support from the NSF Graduate Research Fellowship Program.

REFERENCES

1. Lodge, T. P.; Pudil, B.; Hanley, K. J., The Full Phase Behavior for Block Copolymers in Solvents of Varying Selectivity. *Macromolecules* **2002**, *35*, 4707–4717.

2. Lodge, T. P.; Hanley, K. J.; Pudil, B.; Alahapperuma, V., Phase Behavior of Block Copolymers in a Neutral Solvent. *Macromolecules* **2003**, *36*, 816–822.

3. Nunes, S. P.; Behzad, A. R.; Hooghan, B.; Sougrat, R.; Karunakaran, M.; Pradeep, N.; Vainio, U.; Peinemann, K. V., Switchable pH-Responsive Polymeric Membranes Prepared via Block Copolymer Micelle Assembly. *ACS Nano* **2011,** *5* (5), 3516-3522.

4. Phillip, W. A.; Dorin, R. M.; Werner, J.; Hoek, E. M. V.; Wiesner, U.; Elimelech, M., Tuning Structure and Properties of Graded Triblock Terpolymer-Based Mesoporous and Hybrid Films. *Nano Lett.* **2011,** *11* (7), 2892-2900.

5. Nunes, S. P.; Karunakaran, M.; Pradeep, N.; Behzad, A. R.; Hooghan, B.; Sougrat, R.; He, H. Z.; Peinemann, K. V., From Micelle Supramolecular Assemblies in Selective Solvents to Isoporous Membranes. *Langmuir* **2011,** *27* (16), 10184-10190.

6. Phillip, W. A.; O'Neill, B.; Rodwogin, M.; Hillmyer, M. A.; Cussler, E. L., Self-Assembled Block Copolymer Thin Films as Water Filtration Membranes. *ACS Appl. Mater. Interfaces* **2010,** *2* (3), 847-853.

7. Yang, S. Y.; Ryu, I.; Kim, H. Y.; Kim, J. K.; Jang, S. K.; Russell, T. P., Nanoporous membranes with ultrahigh selectivity and flux for the filtration of viruses. *Adv. Mater.* **2006,** *18* (6), 709-712.

8. van Reis, R.; Zydney, A., Bioprocess membrane technology. *J. Membrane Sci.* **2007,** *297* (1-2), 16-50.

9. Crossland, E. J. W.; Nedelcu, M.; Ducati, C.; Ludwigs, S.; Hillmyer, M. A.; Steiner, U.; Snaith, H. J., Block Copolymer Morphologies in Dye-Sensitized Solar Cells: Probing the Photovoltaic Structure-Function Relation. *Nano Lett.* **2009,** *9* (8), 2813-2819.

10. Singh, M.; Odusanya, O.; Wilmes, G. M.; Eitouni, H. B.; Gomez, E. D.; Patel, A. J.; Chen, V. L.; Park, M. J.; Fragouli, P.; Iatrou, H.; Hadjichristidis, N.; Cookson, D.; Balsara, N. P., Effect of molecular weight on the mechanical and electrical properties of block copolymer electrolytes. *Macromolecules* **2007,** *40* (13), 4578-4585.

11. Yang, S. Y.; Yang, J. A.; Kim, E. S.; Jeon, G.; Oh, E. J.; Choi, K. Y.; Hahn, S. K.; Kim, J. K., Single-File Diffusion of Protein Drugs through Cylindrical Nanochannels. *ACS Nano* **2010,** *4* (7), 3817-3822.

12. Li, X. F.; Fustin, C. A.; Lefevre, N.; Gohy, J. F.; De Feyter, S.; De Baerdemaeker, J.; Egger, W.; Vankelecom, I. F. J., Ordered nanoporous membranes based on diblock copolymers with high chemical stability and tunable separation properties. *J. Mater. Chem.* **2010,** *20* (21), 4333-4339.

13. Yang, S. Y.; Park, J.; Yoon, J.; Ree, M.; Jang, S. K.; Kim, J. K., Virus filtration membranes prepared from nanoporous block copolymers with good dimensional stability under high pressures and excellent solvent resistance. *Adv. Funct. Mater.* **2008,** *18* (9), 1371-1377.

14. Cooney, D. T., Hillmyer, M. A., Cussler, E. L., Moggridge, G. D., Diffusion in nanoporous materials made from block copolymers. *Crystallogr. Rev.* **2006,** *12* (1), 13-24.

15. Phillip, W. A.; Rzayev, J.; Hillmyer, M. A.; Cussler, E. L., Gas and water liquid transport through nanoporous block copolymer membranes. *J. Membrane Sci.* **2006,** *286* (1-2), 144-152.

16. Phillip, W. A.; Amendt, M.; O'Neill, B.; Chen, L.; Hillmyer, M. A.; Cussler, E. L., Diffusion and Flow Across Nanoporous Polydicyclopentadiene-Based Membranes. *ACS Appl. Mater. Interfaces* **2009,** *1* (2), 472-480.

17. Chen, L.; Phillip, W. A.; Cussler, E. L.; Hillmyer, M. A., Robust nanoporous membranes templated by a doubly reactive block copolymer. *J. Am. Chem. Soc.* **2007,** *129* (45), 13786-13787.

18. Peinemann, K. V.; Abetz, V.; Simon, P. F. W., Asymmetric superstructure formed in a block copolymer via phase separation. *Nat. Mater.* **2007,** *6* (12), 992-996.

19. Nunes, S. P.; Sougrat, R.; Hooghan, B.; Anjum, D. H.; Behzad, A. R.; Zhao, L.; Pradeep, N.; Pinnau, I.; Vainio, U.; Peinemann, K. V., Ultraporous Films with Uniform Nanochannels by Block Copolymer Micelles Assembly. *Macromolecules* **2010,** *43* (19), 8079-8085.

CHAPTER 4

Designing Block Copolymer Architectures for Targeted Membrane Performance*

Abstract

Using a combination of block copolymer self-assembly and nonsolvent induced phase separation, isoporous ultrafiltration membranes were fabricated from four poly(isoprene-*b*-styrene-*b*-4-vinylpyridine) triblock terpolymers with similar block volume fractions but varying in total molar mass from 43 kg/mol to 115 kg/mol to systematically study the effect of polymer size on membrane structure. Small-angle X-ray scattering was used to probe terpolymer solution structure in the dope. All four triblocks displayed solution scattering patterns consistent with a body-centered cubic morphology with characteristic spacings increasing with increasing molar mass. After membrane formation, structures were characterized using a combination of scanning electron microscopy and filtration performance tests. Image analysis of scanning electron micrographs of the membrane top surface showed a pore structure consistent with a 2-D square lattice projection in the top thin separation layer. The results of this analysis were used to calculate pore densities that ranged from 1.48×10^{15} to 4.53×10^{14} pores/m^2, which are the highest pore densities yet reported for membranes using self-assembly and nonsolvent induced phase separation. Hydraulic permeabilities ranging from 24 to 850 L m^{-2} hr^{-1} bar^{-1} and pore diameters ranging from 7.3 to 35.5 nm were determined from water permeation at various applied pressures and solute

* Rachel Mika Dorin, William A. Phillip, Hiroaki Sai, Jörg Werner, Menachem Elimelech, and Ulrich Wiesner, Submitted to Chemistry of Materials, April 2013.

rejection tests using single solute polyethylene oxide feed solutions, respectively. Both the hydraulic permeability and pore size increased with increasing molar mass of the parent terpolymer. The combination of polymer characterization and membrane transport tests described here demonstrates the ability to rationally design macromolecular structures to target specific performance characteristics in block copolymer derived ultrafiltration membranes.

Porous polymeric membranes are typically produced using a phase separation technique. This technique involves preparing a casting dope by dissolving a polymer in a solvent, casting the dope into the desired form, allowing solvent to evaporate for a prescribed period of time, and finally precipitating the polymer. Rapid changes in the vapor composition or temperature of the atmosphere surrounding the cast film as well as non-solvent baths are commonly used to precipitate the polymer. Numerous efforts have been made towards the important goal of elucidating the interrelationships between the molecular architecture of the polymer, the membrane structure, and the ultimate performance of membranes obtained from standard phase inversion methods. For example, the effects of adjusting the casting solution composition[1-3], incorporating additives into the dope[4] or phase inversion medium[5], and altering the casting procedure, by changing the casting temperature, evaporation time, and film thickness,[6, 7] have been explored. The effects of polymer molar mass[8] and casting solution viscosity[9] on pore size and pore size distribution have also been studied.

Experimental evidence suggests that, due to this significant effort, the performance of ultrafiltration membranes produced using phase separation methods is reaching an upper limit. At this upper limit, a tradeoff between membrane selectivity

and permeability exists.[10] A similar tradeoff is frequently discussed in the literature on gas phase membrane separations, which is summarized in the "Robeson Plot"[11], as well as reverse osmosis membranes.[12] For ultrafiltration, this performance limit is attributed to the distribution in pore sizes that results from the phase separation methods.[12] For state-of-the-art commercial membranes, the upper bound suggests a normalized pore size deviation of ~20%.[10] Therefore, narrowing the pore size distribution of ultrafiltration membranes is one clear way to produce membranes whose performance could exceed the current performance ceiling. Given the significant efforts dedicated to standard phase inversion methods, accomplishing this goal requires developing new polymer chemistries and processing methodologies.

Significant improvements in the performance potential for ultrafiltration membranes have recently been described through the use of self-assembling block copolymers, which can be applied towards a variety of separation needs, including water purification,[13] drug delivery,[14] and virus filtration.[15, 16] One particularly attractive method for producing membranes with uniform pores and high pore densities, which utilizes a combination of self-assembly and non-solvent induced phase separation (SNIPS),[17] is both scalable and offers impressive separation and permeability profiles. The SNIPS method has been demonstrated with both diblock copolymers[18-23] and triblock terpolymers.[24, 25] Of fundamental importance for advancing SNIPS membranes is an understanding of the relationships between polymer molecular architecture, membrane formation, microstructure, and performance.

The highly controllable architectures of the block copolymers used in the emerging class of SNIPS membranes provide a unique capacity for designing molecules to achieve targeted membrane structures and performance. Herein, we describe the fabrication of several triblock terpolymer SNIPS membranes and investigate the relationship between macromolecular architecture and membrane pore size, pore density, permeability, and solute rejection. We establish clear molecular structure – membrane characteristic correlations that open a path to the molecular design of ultrafiltration membranes.

Results and Discussion

Triblock Terpolymer Characterization. Four poly(isoprene-*b*-styrene-*b*-4-vinylpyridine) (ISV) triblock terpolymers with total molar masses of 43, 77, 91, and 115 kg/mol, abbreviated as ISV43, ISV77, ISV91, and ISV115, respectively, were synthesized using sequential anionic polymerization. From results of earlier studies, volume fractions of 0.30, 0.55, and 0.15 were targeted for the polyisoprene (PI), polystyrene (PS), and poly-4-vinylpyridine (P4VP) blocks, respectively.[24] Experimentally determined volume fractions, f, molar masses, M_n, and polydispersities (PDI) for each triblock terpolymer are summarized in Table 4.1, demonstrating that all four ISVs are similar in composition.

Transmission electron microscopy (TEM) micrographs of polymer films cast from chloroform and allowed to dry slowly show bulk morphologies of the self-assembled polymers (Figure 4.1). The top row of micrographs in Figure 4.1 shows samples stained with I_2 (g), which is selective for the P4VP block. Images of ISV43, ISV77, and ISV91 (Figures 4.1a, 4.1b, and 4.1c) are consistent with periodic, ordered

P4VP cylinders; the larger molar mass ISV115 exhibits TEM projections consistent with disordered P4VP micelles (Figure 4.1d). The bottom row shows micrographs of the same polymer samples stained with OsO_4 (g), which is selective for the PI block. In these images, the PI in ISV43, ISV77, and ISV91 (Figures 4.1e, 4.1f, and 4.1g) forms an interconnected honeycomb structure, whereas for ISV115 the results show a disordered interconnected PI network (Figure 4.1h).

The morphology of the bulk films was further investigated with small-angle X-ray scattering (SAXS), as shown in Figure 4.2. Consistent with the ordered structures seen in TEM for ISV43, ISV77, and ISV91, the SAXS patterns of these films can be indexed with a 2-D hexagonal morphology with channel-to-channel spacings (i.e. $\frac{4\pi}{\sqrt{3}q^*}$, where q^* is the reciprocal-space length corresponding to the first order peak) of 43 nm, 64 nm, and 73 nm, respectively. The SAXS pattern for ISV115 (Figure 4.2, top curve) shows a broad first order peak, but no well-developed higher order peaks and can thus not be indexed with a typical block copolymer lattice, suggesting a locally microphase-separated nanostructure. The value of q^* for the ISV115 pattern gives a characteristic length of 60 nm in the sample. The channel-to-channel spacing for the three smaller polymers increases with increasing molar mass, as expected; however, that trend does not continue with the largest ISV115 triblock, likely due to the morphological change from the ordered 2-D hexagonal lattice to the disordered micellar structure as observed in TEM.

Triblock Terpolymer Solution Structure. The SNIPS technique was used to transform self-assembling block copolymers into asymmetric porous membranes.[17]

This method produces a film comprising a thin (~50-200 nm) selective top layer of uniform, self-assembled pores above a macroporous support layer that is typically tens of micrometers thick. The SNIPS procedure is similar to standard phase inversion methods; however, the use of block copolymers, which self-assemble during the evaporation step, produces a membrane with a unique isoporous separation layer.

Recent work using SAXS suggested that solutions of both diblocks and triblocks in specific casting solvents contained ordered structures at elevated concentrations.[17] It was found that using the SNIPS method with casting solutions at concentrations slightly below where ordered structures were observed produced membranes with the desired asymmetric structure (i.e. a thin isoporous separation layer above a microporous substructure). In addition to guiding the selection of the casting solution composition, terpolymer ordering in solution was indicative of the pore geometry and density in the final membrane. In light of this discovery, SAXS was performed on solutions of the ISV43, ISV77, ISV91, and ISV115 polymers dissolved in a mixture of the casting solvents 1,4-dioxane (DOX) and tetrahydrofuran (THF). The solvents were mixed at a ratio of 7:3 by weight. Figure 4.3 shows the resulting SAXS patterns for ISV43 at 24 wt% and ISV77, ISV91, and ISV115 at 16 wt%, which are all consistent with a body-centered cubic (BCC) structure with $(q/q^*)^2$=1, 2, 3, 4, 5, 6, and 7. The corresponding lattice constants were 38, 57, 60, and 73 nm for ISV43, ISV77, ISV91, and ISV115, respectively.

Interestingly, the SAXS pattern of the ISV115 sample in solution is consistent with a well-ordered BCC structure despite the disordered micelles seen in the TEM of the bulk material (Figure 4.1h). Indeed, this sample, as well as samples ISV77 and

ISV91, exhibit six distinguishable higher order reflections, including reflections at $(q/q^*)^2=7$, which excludes the lattice assignment to simple cubic. The existence of ordered solution structures suggests that the organic solvents in the casting solution, even at high polymer concentrations (i.e. 16 wt%), mobilize the polymer chains sufficiently for re-organization into highly periodic structures. Furthermore, the solution SAXS guided selection of the initial polymer concentration in the casting dopes for all terpolymer membranes produced through the SNIPS technique.[17]

Membrane Fabrication and Structural Characterization. SEM micrographs of the top surfaces and cross sections of membranes fabricated from the ISV triblocks are shown in Figure 4.4. A DOX/THF solvent ratio of 7/3 by weight, an evaporation period of 75 s, and polymer concentrations of 16, 12, and 11 wt% were used to fabricate membranes from the ISV43, ISV77, and ISV91 terpolymers, respectively. ISV115 membranes were cast from a 9 wt% solution using a DOX/THF solvent ratio of 6/4 and an evaporation period of 45 s. The polymer concentrations used were selected to yield casting dopes sufficiently viscous for the doctor blade procedure, while remaining below the concentration at which solution structure is seen, as described previously.[17]

The conditions used to fabricate membranes from ISV115 resulted in membranes with the most consistent top structure, as determined from SEM imaging. However, visual inspection of the top surface (Figure 4.4d) indicates that the pore density is lower, the pore size distribution is broader, and the pore packing is less ordered than for membranes obtained from the smaller polymers. Additionally, ISV115 membranes cast from a 7/3 DOX/THF solvent ratio and an evaporation period

of 75 s from a 9 wt% solution (i.e. conditions chosen for all other membrane formation processes), resulted in only partially open pores that were randomly distributed across the membrane surface, reminiscent of the bulk structure of the polymer (see Appendix C, Figure C.1). We speculate that the optimized conditions with increased THF content used in the casting solution (THF is a better solvent for the ISV triblock than DOX), as well as a shorter evaporation period, contribute to a membrane separation structure closer to the structure of the casting solution than to that of the disordered bulk material. Given the large phase space applicable to the SNIPS technique, further exploration into the casting solution (e.g. polymer architecture, concentration, and solvent composition) as well as the casting procedure (e.g. casting environment, thickness, evaporation period, and coagulation bath composition) may reveal additional conditions that produce membranes with the desired structure and enhanced performance.

The SEM micrographs in Figure 4.4 show that the membranes exhibit a 2-D square pore lattice and a separation layer thickness of ~100-200 nm. FFT image analysis of the top surface SEM images corroborates the square pore geometry (Figure 4.5). Given the 2-D square lattice of the pores, pore-to-pore distances of 26, 44, 45, and 47 nm and pore densities of 1.5×10^{15}, 5.2×10^{14}, 4.9×10^{14}, and 4.5×10^{14} pores/m^2 were calculated for the ISV43, ISV77, ISV91, and ISV115 samples, respectively, as summarized in Table 4.2. The pore densities of these membranes are over an order of magnitude greater than any similarly produced diblock copolymer SNIPS membrane to date. This can be attributed to the use of lower molar mass polymers, which also allows access to smaller pore dimensions, *vide infra*. In turn, this

is enabled in part by the low glass transition (T_g) polyisoprene block, which provides the membranes with increased toughness despite the typical brittleness observed for low molar mass polystyrene materials (see also remarks in next section).[24]

Membrane Performance. Deionized (DI) water flux through the membranes was measured at applied pressures between 20.7 and 137.9 kPa (3 and 20 psig) using a pressurized stirred cell. Pure water permeabilities of 24, 154, 196, and 850 L m^{-2} hr^{-1} bar^{-1} for the ISV43, ISV77, ISV91, and ISV115 membranes, respectively, were calculated using the slope of the measured water flux vs. applied pressure (data not shown). The reported values, which are summarized in Table 4.2, are an average of at least three measurements on pristine membranes, with the exception of the ISV43 material. Membranes fabricated from ISV43 were relatively brittle due to the low molar mass of the polymer resulting in limited entanglement between polymer chains. As such, only two ISV43 membranes were successfully tested. The challenges associated with fabricating and handling the small molar mass ISV43 membrane, despite the presence of the toughness enhancing PI component, implies a lower limit to the membrane pore size that can be achieved using an unmodified ISV terpolymer. Mechanical strength may be improved through the use of support membranes, bridging rubbery polymers to increase toughness,[26] or post-fabrication procedures, such as cross-linking the matrix block(s)[27] or polymeric coatings.[28]

Aqueous solutions containing PEO molecules ranging in molar mass from 4 to 203 kg/mol were used to test the ability of the ISV-derived membranes to reject dissolved solutes. The results of these experiments are shown in Figure 4.6. For a given PEO molar mass (i.e., solute size), membranes fabricated from lower molar

mass ISV samples exhibited greater solute rejection, which manifests itself as a horizontal shift of the molecular weight cut-off (MWCO) curve. This dependence of solute rejection on the molecular architecture of the parent terpolymer demonstrates the ability to tune a key membrane property through rational macromolecular design.

The solute rejection data producing the MWCO curves were used to calculate the membrane pore size by comparing actual solute rejection (i.e., the observed rejection corrected for concentration polarization) to the solute rejection predicted by the hindered transport model developed by Zeman and Wales[29]:

$$R = 1 - \left[(1-\lambda)^2\left[2-(1-\lambda)^2\right]\exp\left(-0.7146\lambda^2\right)\right] \quad (1)$$

In this expression, the solute rejection, R, is a function of λ, where λ is defined as the ratio of the characteristic solute size to the pore diameter (d_{pore}). Here, two times the hydrodynamic radius of the PEO molecule, which was determined from tracer diffusion data,[30] is taken as the characteristic solute size. The residual squares of the actual and predicted rejections from eq 1 were then minimized to determine d_{pore}. This yielded pore sizes of 7.3, 15.9, 17.1, and 35.5 nm for the ISV43, ISV77, ISV91, and ISV115 membranes, respectively, as summarized in Table 4.2. The solute rejection data clearly demonstrate pore sizes that increase with increasing polymer molar mass; this observation is consistent with the pure water permeabilities. The small pore sizes found here are the smallest reported for SNIPS membranes to date, which is directly related to the relatively low molar mass triblock terpolymers used. These small pore sizes could enable small solute separations without the need for membrane post-modifications.

It is worth noting that for ISV77 and ISV91 the pore diameters calculated from solute rejection data are similar. This is consistent with the FFT analysis of membrane top surfaces, which revealed similar pore-to-pore distances (Figure 4.5), as well as the solution SAXS data, which showed similar characteristic length scales (Figure 4.3). We attribute this to the fact that even though ISV77 and ISV91 have a 15 kg/mol difference in total molar mass, the P4VP component in both polymers is 12.7 kg/mol. This suggests that in the casting solution, the size of the swollen P4VP appears to have a greater effect on the pore size in the ultimate membrane than the molar mass of the PI and PS components for these two polymers. It also reiterates the findings of an earlier publication[17] that suggest solution SAXS is a valuable tool that can help guide the casting conditions used for the SNIPS process, and demonstrates the precise control over pore size possible through block copolymer design.

In summary, the SNIPS process was used to fabricate membranes from ISV triblock terpolymers ranging in total molar mass from 43 to 115 kg/mol. Investigations into the bulk structure of the triblock material revealed that both hexagonal and disordered micellar morphologies led to solution ordering and successful SNIPS membranes, which expands the applicable phase space of block copolymers for membrane fabrication. Increasing the molar mass of the terpolymer resulted in membranes with lower pore densities and larger pore diameters for the ISV compositions used in this study. Evidence of these structural changes was observed in the water and solute transport characteristics of the various ISV membranes. Membranes fabricated from higher molar mass samples of ISV produced higher water fluxes and membranes formed from lower molar mass samples rejected dissolved

solutes to a higher degree. Utilizing the low molar mass, 43 kg/mol ISV terpolymer, provided access to the smallest pore size (7.3 nm) and the highest pore density (>10^{15} pores/m^2) yet achieved for SNIPS membranes, which will facilitate small solute separations without post-functionalization procedures. The greater understanding of the relationship between molecular block copolymer architecture and membrane structure and performance developed in this study suggests that by tailoring the molar mass of the ISV terpolymer, the structure and performance of the resulting SNIPS membranes can be systematically tuned for specific applications.

Methods

Polymer Synthesis and Characterization. Poly(isoprene-*b*-styrene-*b*-4-vinylpyridine) (ISV) triblock terpolymers were synthesized via sequential anionic polymerization as previously reported.[24] The molar mass of three polymers, ISV43, ISV77, and ISV115, was determined using a combination of ^{1}H solution nuclear magnetic resonance (^{1}H NMR) and gel permeation chromatography (GPC) in tetrahydrofuran (THF) as a solvent on a Water 510 GPC instrument equipped with a Water 2410 differential refractive index detector. Volume fractions of each block were calculated using ^{1}H NMR spectra obtained on a Varian INOVA 400 MHz spectrometer using $CDCl_3$ (δ=7.27 ppm) signal as an internal standard. The ^{1}H NMR was also used to determine the molar mass and volume fractions of ISV91 using the signal for the *sec*-butyllithium initiator as a reference. The ^{1}H NMR method of determining molar mass was found to be within 5% of GPC methods. Bulk films of ISV were prepared by dissolving the polymer in chloroform at <5 wt% and pouring the solution into a Teflon dish. The dish was covered with a glass dome to slow

solvent evaporation, and the chloroform was evaporated overnight. Small-angle X-ray scattering (SAXS) on bulk samples was performed at the G1 station of the Cornell High Energy Synchrotron Source (CHESS) with a 250 cm flight path and an X-ray energy ranging from 8-10.6 keV. Two-dimensional patterns obtained on a phosphor-optical fiber coupled CCD were azimuthally integrated to generate the 1D SAXS patterns in the MATLAB software suite.[31] The scattering vector, q, is defined as $q = \frac{4\pi}{\lambda}\sin\theta$, where θ is half of the total scattering angle. Bulk samples were sectioned at 50-70 nm using a Leica Ultracut UC7 cryo-ultramicrotome at -60 °C. Microtomed samples were selectively stained with either OsO_4 (g) for 30 minutes or with I_2 (g) for 2 hours. Bright field TEM (BF-TEM) images were obtained using a FEI Tecnai F12 Spirit electron microscope equipped with a SIS Megaview III CCD camera, operated at an acceleration voltage of 120 kV.

Solution preparation and characterization. Solutions of ISV for SAXS and for membrane fabrication were prepared by first mixing 1,4-dioxane (DOX) and THF and subsequently dissolving the polymer in the solvent mixture overnight. Solutions for SAXS were centrifuged into 0.9-1.0 mm glass capillaries (Charles-Supper Co.) and flame sealed. SAXS data were taken at the CHESS beamline.

Membrane preparation and characterization. Membranes were hand-cast using a doctor blade (Testing Machines, Inc., K Control Coater) with a gate height of 200 μm, evaporated for a specified time (see main text), and plunged into deionized (DI) water. Membranes were dipped in ethanol, dried under ambient conditions, and coated with gold-palladium prior to SEM imaging, which was performed on either a Hitachi Ultra-

High Resolution Analytical Field Emission Scanning Electron Microscope (FE-SEM) SU-70 or a Zeiss Leo 1550 FE-SEM. Membrane hydraulic permeability and solute rejection experiments were conducted in a stirred cell (Amicon 8010, Millipore Co.) pressurized with N_2 (g). Solute rejection tests were performed using single solute polyethylene oxide (PEO) solutions at a concentration of 1 g/L in DI water. PEO concentration in the feed and permeate were determined using a Shimadzu total organic carbon analyzer or a TA Instruments thermogravimetric analyzer Q500. Permeate water flux and PEO rejection measurements were run at applied pressure drops ranging from 20.7 to 137.9 kPa (3 to 20 psig) to maintain similar hydrodynamic conditions between samples.

Acknowledgements

This publication is based on work supported by award No. KUS-C1-018-02, made by King Abdullah University of Science and Technology (KAUST). R.M.D. acknowledges support from the NSF Graduate Research Fellowship Program (GRFP). H.S. acknowledges funding by the NSF single investigator award (DMR-1104773). This work made use of the Cornell Center for Materials Research Shared Facilities, which are supported through the NSF MRSEC program (DMR-1120296) and the Cornell High Energy Synchrotron Source (CHESS), which is supported by the NSF & NIH/NIGMS via NSF award DMR-0936384, and MacCHESS supported by NIGMS award GM-103485. We thank J. Weidman for SEM cross-sectional analysis of the ISV43 membrane.

Table 4.1 Volume fractions (f), molar masses (M_n), and polydispersities (PDI) of each block of the four ISV triblock terpolymers used in this study

	f_{PI}	f_{PS}	f_{P4VP}	M_n (kg/mol)	PDI
ISV43	0.27	0.55	0.18	43	1.02
ISV77	0.29	0.57	0.14	77	1.16
ISV91	0.32	0.55	0.13	91	1.20
ISV115	0.29	0.58	0.13	115	1.12

Table 4.2 Structural and performance characteristics of ISV43, ISV77, ISV91, and ISV115 triblock terpolymer membranes.

	Pore-to-pore distance[a] (nm)	Pore density (pores/m^2)	Permeability ($Lm^{-2}hr^{-1}bar^{-1}$)	d_{pore}[b] (nm)
ISV43	26	1.48×10^{15}	24	7.3
ISV77	44	5.17×10^{14}	154	15.9
ISV91	45	4.94×10^{14}	196	17.1
ISV115	47	4.53×10^{14}	850	35.5

[a] as determined by Fourier analysis of SEM images of membrane top surface.

[b] as determined by single solute rejection tests.

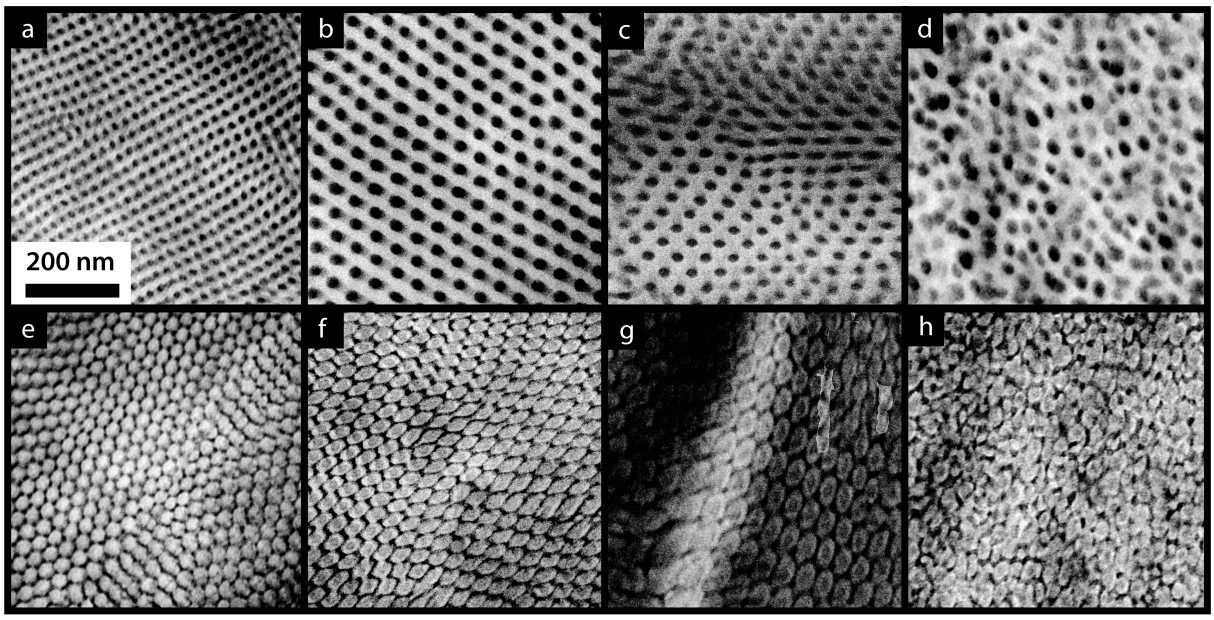

Figure 4.1 TEM images of bulk ISV stained with I_2 (g), which is selective for poly-(4-vinylpyridine) (top row) and OsO_4 (g), which is selective for polyisoprene (bottom row). (a,e) ISV43, (b,f) ISV77, (c,g) ISV91, and (d,h) ISV115. Scale bar is 200 nm and all images are at the same magnification.

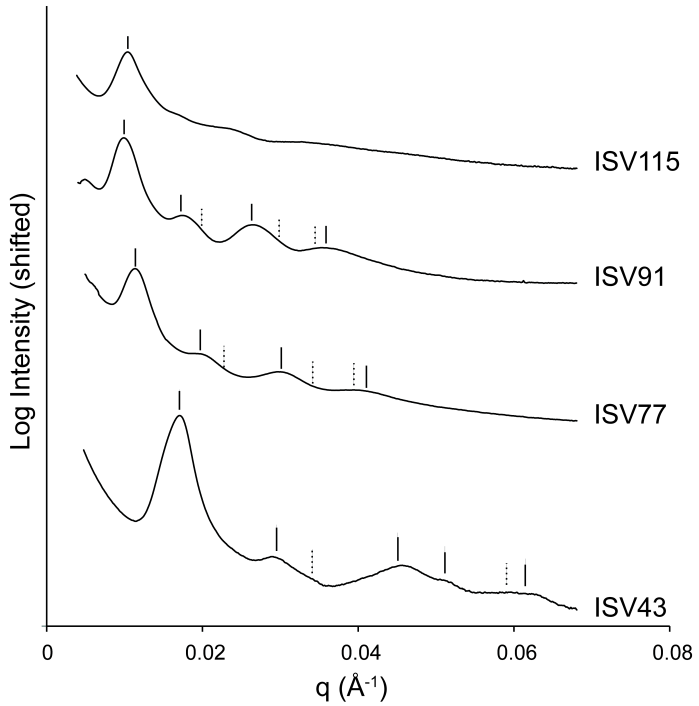

Figure 4.2 SAXS patterns for bulk ISV triblock terpolymers cast from chloroform. ISV43, ISV77, and ISV91 exhibit SAXS patterns consistent with a hexagonal morphology (dashes correspond to expected peak positions for a hexagonal structure with $(q/q^*)^2$=1, 3, 4, 7, 9, 12, and 13, with q^* equal to the position of the first order peak). Channel-to-channel spacings correspond to 43, 64, and 73 nm for ISV43, ISV77, and ISV91, respectively. The characteristic length scale of ISV115, which cannot be indexed to a simple block copolymer lattice, is 60 nm from the position of q^*.

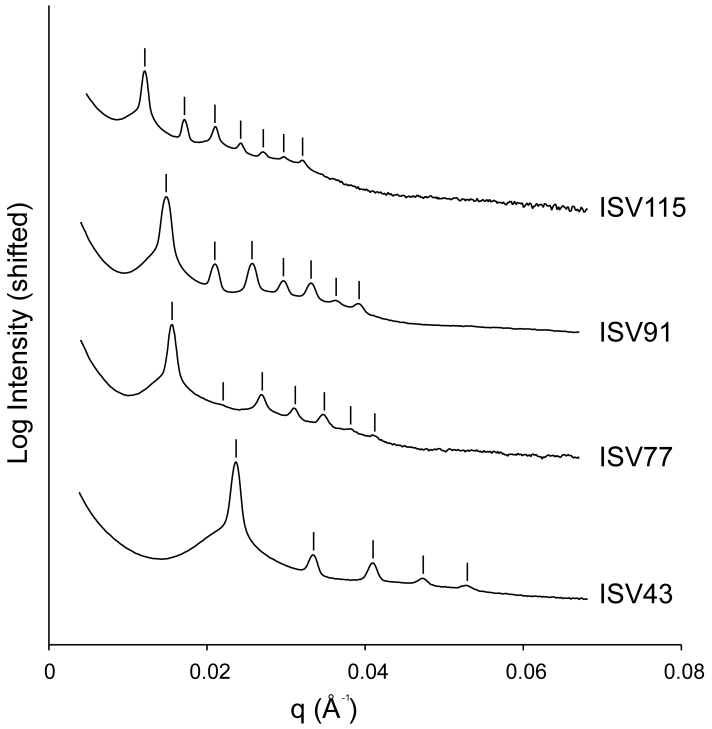

Figure 4.3 SAXS from solutions of ISVs in 7/3 DOX/THF. Dashes correspond to $(q/q^*)^2$=1, 2, 3, 4, 5, 6, and 7, consistent with expected peak positions for an ordered BCC lattice. Polymer concentrations and lattice constants are 24 wt% and 38 nm, 16 wt% and 57 nm, 16 wt% and 60 nm, and 16 wt% and 73nm for ISV43, ISV77, ISV91, and ISV115, respectively.

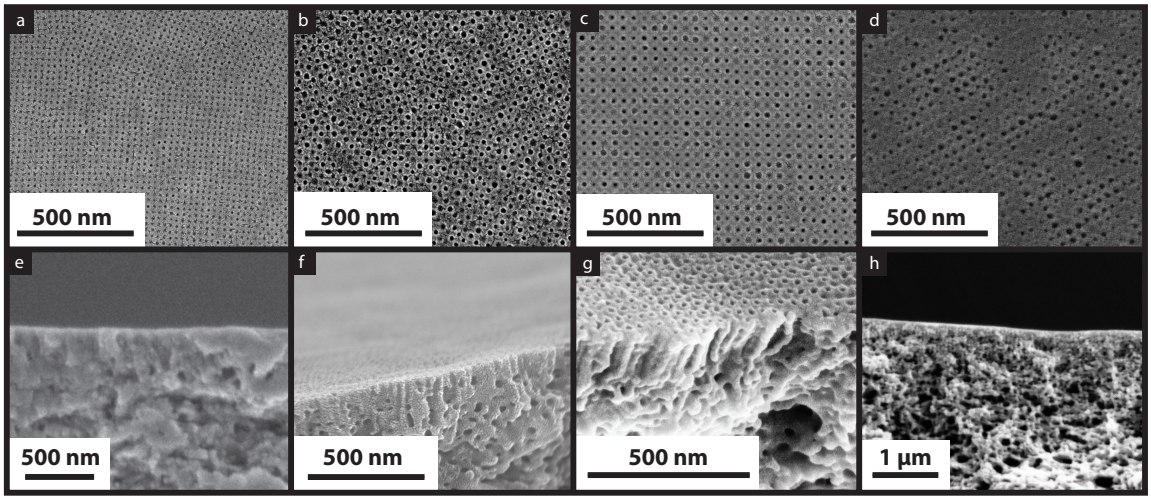

Figure 4.4 SEM characterization of top surfaces (top row) and cross sections (bottom row) of ISV membranes. (a,e) ISV43, (b,f) ISV77, (c,g) ISV91, and (d,h) ISV115. ISV43, ISV77, and ISV91 were prepared using a solvent ratio of 7/3 DOX/THF and an evaporation period of 75 s, while ISV115 was prepared using a solvent ratio of 6/4 DOX/THF and an evaporation period of 45 s.

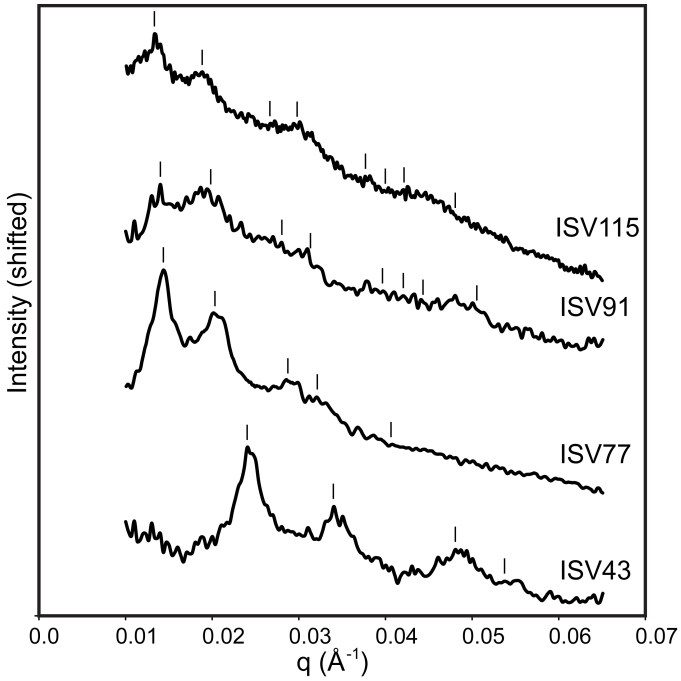

Figure 4.5 FFT image analysis of SEM images of the top surface of membranes confirms a 2D square pore geometry for: (a) ISV43, (b) ISV77, (c) ISV91 and (d) ISV115. Dashes indicate expected peak positions up to $(q/q^*)^2$=1, 2, 4, 5, 8, 9, 10, and 13, for 2D square lattices. q^* positions yield pore-to-pore distances of 26, 44, 45, and 47 nm for ISV43, ISV77, ISV91, and ISV115 membranes, respectively.

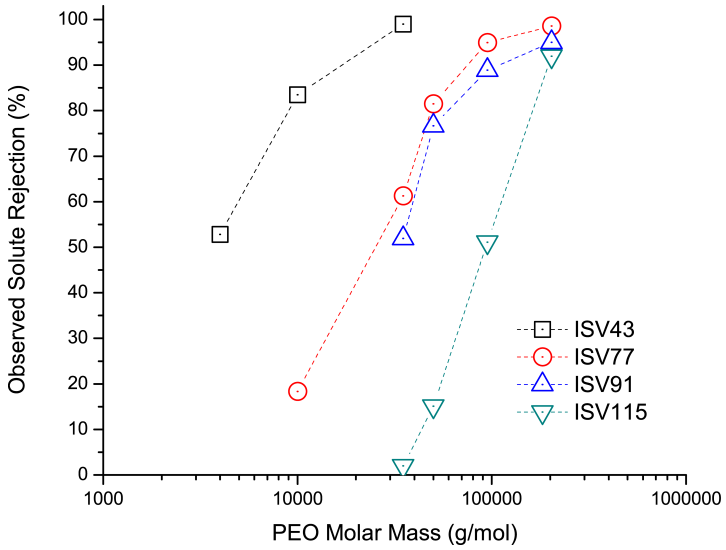

Figure 4.6 Membranes were challenged with polyethylene oxide (PEO) molecules of varying molar mass dissolved in DI water at 1 g/L. Molecular weight cutoff curves are shown for ISV43 (black squares), ISV77 (red circles), ISV91 (blue triangles), and ISV115 (green inverted triangles).

REFERENCES

1. Nguyen, T. D.; Matsuura, T.; Sourirajan, S., Effect of the Casting Solution Composition on Pore Size and Pore Size Distribution of Resulting Aromatic Polyamide Membranes. *Chemical Engineering Communications* **1987,** *57* (1-6), 351-369.

2. Barth, C.; Goncalves, M. C.; Pires, A. T. N.; Roeder, J.; Wolf, B. A., Asymmetric Polysulfone and Polyethersulfone Membranes: Effects of Thermodynamic Conditions During Formation on Their Performance. *Journal of Membrane Science* **2000,** *169* (2), 287-299.

3. Ahmad, A. L.; Sarif, M.; Ismail, S., Development of an Integrally Skinned Ultrafiltration Membrane for Wastewater Treatment: Effect of Different Formulations of PSf/NMP/PVP on Flux and Rejection. *Desalination* **2005,** *179*, 257-263.

4. Lafreniere, L. Y.; Talbot, F. D. F.; Matsuura, T.; Sourirajan, S., Effect of Poly(vinylpyrrolidone) Additive on the Performance of Poly(ether sulfone) Ultrafiltration Membranes. *Industrial & Engineering Chemistry Research* **1987,** *26* (11), 2385-2389.

5. Nguyen, T. D.; Matsuura, T.; Sourirajan, S., Effect of Nonsolvent Additives on the Pore-Size and the Pore-Size Distribution of Aromatic Polyamide RO Membranes. *Chemical Engineering Communications* **1987,** *54* (1-6), 17-36.

6. Kunst, B.; Sourirajan, S., Effect of Casting Conditions on the Performance of Porous Cellulose Acetate Membranes in Reverse Osmosis. *Journal of Applied Polymer Science* **1970,** *14* (3), 723-733.

7. Bartels, C. R.; Kreuz, K. L.; Wachtel, A., Structure-Performance Relationships of Composite Membranes: Porous Support Densification. *Journal of Membrane Science* **1987,** *32* (2-3), 291-312.

8. Miyano, T.; Matsuura, T.; Sourirajan, S., Effect of Polymer Molecular Weight, Solvent and Casting Solution Composition on the Pore Size and the Pore Size Distribution of Polyethersulfone (Victrex) Membrane. *Chemical Engineering Communications* **1990,** *95* (1), 11-26.

9. Nguyen; D., T.; Chan, K.; Matsuura; T.; Sourirajan; S., Viscoelastic and Statistical Thermodynamic Approach to the Study of the Structure of Polymer Film Casting Solutions for Making RO/UF Membranes. *Anglais* **1985,** *24* (4), 655-665.

10. Mehta, A.; Zydney, A. L., Permeability and Selectivity Analysis for Ultrafiltration Membranes. *Journal of Membrane Science* **2005,** *249* (1-2), 245-249.

11. Robeson, L. M., Correlation of Separation Factor Versus Permeability for Polymeric Membranes. *Journal of Membrane Science* **1991,** *62* (2), 165-185.

12. Geise, G. M.; Park, H. B.; Sagle, A. C.; Freeman, B. D.; McGrath, J. E., Water Permeability and Water/Salt Selectivity Tradeoff in Polymers for Desalination. *Journal of Membrane Science* **2011,** *369*, 130-138.

13. Shannon, M. A.; Bohn, P. W.; Elimelech, M.; Georgiadis, J. G.; Marinas, B. J.; Mayes, A. M., Science and Technology for Water Purification in the Coming Decades. *Nature* **2008,** *452* (7185), 301-310.

14. Yang, S. Y.; Yang, J.-A.; Kim, E.-S.; Jeon, G.; Oh, E. J.; Choi, K. Y.; Hahn, S. K.; Kim, J. K., Single-File Diffusion of Protein Drugs through Cylindrical Nanochannels. *ACS Nano* **2010,** *4* (7), 3817-3822.

15. Yang, S. Y.; Ryu, I.; Kim, H. Y.; Kim, J. K.; Jang, S. K.; Russell, T. P., Nanoporous Membranes with Ultrahigh Selectivity and Flux for the Filtration of Viruses. *Advanced Materials* **2006,** *18* (6), 709-712.

16. Yang, S. Y.; Park, J.; Yoon, J.; Ree, M.; Jang, S. K.; Kim, J. K., Virus Filtration Membranes Prepared from Nanoporous Block Copolymers with Good Dimensional Stability under High Pressures and Excellent Solvent Resistance. *Advanced Functional Materials* **2008,** *18* (9), 1371-1377.

17. Dorin, R. M.; Marques, D. S.; Sai, H.; Vainio, U.; Phillip, W. A.; Peinemann, K. V.; Nunes, S. P.; Wiesner, U., Solution Small-Angle X-ray Scattering as a Screening and Predictive Tool in the Fabrication of Asymmetric Block Copolymer Membranes. *Acs Macro Letters* **2012,** *1* (5), 614-617.

18. Peinemann, K. V.; Abetz, V.; Simon, P. F., Asymmetric Superstructure Formed in a Block Copolymer viaPhase Separation. *Nat Mater* **2007,** *6* (12), 992-996.

19. Nunes, S. P.; Sougrat, R.; Hooghan, B.; Anjum, D. H.; Behzad, A. R.; Zhao, L.; Pradeep, N.; Pinnau, I.; Vainio, U.; Peinemann, K. V., Ultraporous Films with Uniform Nanochannels by Block Copolymer Micelles Assembly. *Macromolecules* **2010,** *43* (19), 8079-8085.

20. Nunes, S. P.; Behzad, A. R.; Hooghan, B.; Sougrat, R.; Karunakaran, M.; Pradeep, N.; Vainio, U.; Peinemann, K. V., Switchable pH-Responsive Polymeric

Membranes Prepared via Block Copolymer Micelle Assembly. *ACS Nano* **2011,** *5* (5), 3516-3522.

21. Nunes, S. P.; Karunakaran, M.; Pradeep, N.; Behzad, A. R.; Hooghan, B.; Sougrat, R.; He, H. Z.; Peinemann, K. V., From Micelle Supramolecular Assemblies in Selective Solvents to Isoporous Membranes. *Langmuir* **2011,** *27* (16), 10184-10190.

22. Jung, A.; Rangou, S.; Abetz, C.; Filiz, V.; Abetz, V., Structure Formation of Integral Asymmetric Composite Membranes of Polystyrene-block-Poly(2-vinylpyridine) on a Nonwoven. *Macromolecular Materials and Engineering* **2012,** *297* (8), 790-798.

23. Hahn, J.; Filiz, V.; Rangou, S.; Clodt, J.; Jung, A.; Buhr, K.; Abetz, C.; Abetz, V., Structure Formation of Integral-Asymmetric Membranes of Polystyrene-block-Poly(ethylene oxide). *Journal of Polymer Science Part B: Polymer Physics* **2013,** *51* (4), 281-290.

24. Phillip, W. A.; Dorin, R. M.; Werner, J.; Hoek, E. M.; Wiesner, U.; Elimelech, M., Tuning Structure and Properties of Graded Triblock Terpolymer-Based Mesoporous and Hybrid Films. *Nano Lett* **2011,** *11* (7), 2892-2900.

25. Jung, A.; Filiz, V.; Rangou, S.; Buhr, K.; Merten, P.; Hahn, J.; Clodt, J.; Abetz, C.; Abetz, V., Formation of Integral Asymmetric Membranes of AB Diblock and ABC Triblock Copolymers by Phase Inversion. *Macromolecular Rapid Communications* **2013,** *[Online early access]* (DOI: 10.1002/marc.201200770. Published Online: Feb 7, 2013).

26. Jackson, E. A.; Lee, Y.; Hillmyer, M. A., ABAC Tetrablock Terpolymers for Tough Nanoporous Filtration Membranes. *Macromolecules* **2013**.

27. Chen, L.; Phillip, W. A.; Cussler, E. L.; Hillmyer, M. A., Robust Nanoporous Membranes Templated by a Doubly Reactive Block Copolymer. *Journal of the American Chemical Society* **2007,** *129* (45), 13786-13787.

28. Clodt, J. I.; Filiz, V.; Rangou, S.; Buhr, K.; Abetz, C.; Höche, D.; Hahn, J.; Jung, A.; Abetz, V., Double Stimuli-Responsive Isoporous Membranes via Post-Modification of pH-Sensitive Self-Assembled Diblock Copolymer Membranes. *Advanced Functional Materials* **2012**.

29. Zeman, L.; Wales, M., Polymer Solute Rejection by Ultrafiltration Membranes. *Synthetic Membranes: Vol. II, American Chemical Society: Washington, DC* **1981,** *154*, 411-434.

30. Faraone, A.; Magazu, S.; Maisano, G.; Migliardo, P.; Tettamanti, E.; Villari, V., The Puzzle of Poly(ethylene oxide) Aggregation in Water: Experimental Findings. *Journal of Chemical Physics* **1999,** *110* (3), 1801-1806.

31. Finnefrock, A. C.; Ulrich, R.; Toombes, G. E. S.; Gruner, S. M.; Wiesner, U., The Plumber's Nightmare: A New Morphology in Block Copolymer-Ceramic Nanocomposites and Mesoporous Aluminosilicates. *Journal of the American Chemical Society* **2003,** *125* (43), 13084-13093.

CHAPTER 5

Mechanistic Study of High Performance Triblock Terpolymer SNIPS Membrane Formation via In Situ GISAXS.*

Abstract

In situ block copolymer membrane formation that relies on self-assembly of doctor bladed solutions was observed using grazing incidence small-angle X-ray scattering (GISAXS). The evaporation dependent evolution of a disordered to an ordered structure in a film of the triblock terpolymer poly(isoprene-*b*-styrene-*b*-4-vinyl pyridine) dissolved in 1,4-dioxane and tetrahydrofuran was observed. The GISAXS pattern of the film exhibited Bragg spots consistent with a *bcc* structure between evaporation times of 37 s and 58 s, with the most intense Bragg spots occurring after 46 s of evaporation. Projections of the GISAXS patterns were consistent with solution small angle X-ray scattering. Such in situ methods offer the potential to optimize the key parameter of evaporation time in the production of isoporous integral block copolymer membranes.

The application of block copolymer self-assembly towards membrane separations has received significant attention over the past several years due to the potential for significantly improved performance. In particular, the combination of self-assembly and non-solvent induced phase separation (SNIPS)[1] produces integral isoporous membranes. Using this facile and industrially scalable method, membranes have been fabricated from a variety of block copolymers,

* Rachel Mika Dorin, Detlef-M. Smilgies, Yibei Gu, and Ulrich Wiesner, to be submitted

including poly(styrene-*b*-4-vinyl pyridine),[2] poly(styrene-*b*-2-vinyl pyridine),[3] poly(styrene-*b*-ethylene oxide),[4] poly(styrene-*b*-2-vinyl pyridine-*b*-ethylene oxide),[5] and poly(isoprene-*b*-styrene-*b*-4-vinyl pyridine).[6] These SNIPS membranes exhibit exceptional fluxes and high-resolution separations, as well as the capacity for post-functionalization, leading to temperature-dependent performance[7] and charge-based separations[8].

Results and Discussion

SNIPS membrane are typically prepared by casting a film of block copolymer solution via doctor blade on a substrate, allowing the film to evaporated for a specified period of time, and finally plunging the film into a non-solvent bath. Meaningful progress towards membrane fabrication has clearly been achieved. However, a fundamental understanding of the formation mechanism has yet to be fully revealed. The vast majority of mechanistic studies on SNIPS membrane systems to date have relied on *ex situ* measurements to elucidate possible formation mechanisms, from solution small-angle X-ray scattering,[1] cryo-electron microscopy,[9,10,11] small-angle neutron scattering,[10] and transmission electron microscopy tomography.[12] While grazing incidence small-angle X-ray scattering (GISAXS) has been used as tool for investigating block copolymer morphologies and morphological transitions via solvent swelling,[13, 14] this method has yet to be applied to doctor bladed block copolymer solutions. Here we report for the first time *in situ* GISAXS measurement on triblock terpolymer SNIPS membrane casting solutions during the formation process. Through time-resolved GISAXS on doctor-bladed solutions of poly(isoprene-*b*-styrene-*b*-4-vinyl pyridine) (ISV), order-disorder transition (ODT) during the key evaporative step

was observed. Both the film morphology and the time interval over which the surface structure developed were consistent with previous *ex situ* experiments on this ISV membrane system.

In situ GISAXS experiments were performed on a custom-built doctor blade setup in the D1 line at the Cornell High Energy Synchrotron Source (CHESS), as detailed by Smilgies *et al*.[15] The triblock terpolymer had a total molar mass of 43 kg/mol and volume fractions of 0.27, 0.55, and 0.18 for the polyisoprene, polystyrene, and poly-4-vinyl pyridine components, respectively, and is labeled ISV43. A solution of 20 wt% ISV43 in 1,4-dioxane (DOX) and tetrahydrofuran (THF) (7/3 by weight) was spread via a doctor blade across a glass slide. GISAXS patterns were collected on a CCD detector every 4-5 s, starting immediately after the spreading. A diagram of the experimental setup is shown in Figure 5.1. An incidence angle, α, of 0.12° and a sample-to-detector distance of 1.85 m was used. The gate height of the doctor blade was 200 μm, and the casting speed was 1.75 cm/s. This system was chosen because triblock terpolymers of similar composition in the same solvent system successfully resulted in isoporous, high performance membranes via the SNIPS process.[1, 6]

Using this *in situ* GISAXS method, the evolution from a non-periodic structure to a structure consistent with a *bcc* morphology was observed. 2D GISAXS patterns of the film at 0 s, 25 s, 46 s, and 62 s are shown in Figure 5.2a, 5.2b, 5.2c, and 5.2d, respectively. The GISAXS patterns exhibit two rings, one at lower and one at higher q_z values. We expect that the incident angle is between the critical angle of the film and the substrate, causing the reflected intensity seen as the upper ring. The diffuse rings observed at 0 s of evaporation and the similar higher intensity rings seen at 25 s of

evaporation indicate a phase separated but disordered structure. At an evaporation time of 46 s that the most intense and discrete Bragg spots emerge, indicating the existence of an ordered solution at the film surface. After 62 s of evaporation, the Bragg spots disappear and the GISAXS pattern again displays a non-periodic solution structure.

Analysis of the spot pattern after 46 s of evaporation is shown in Figure 5.3. The circles and crosses mark expected peak positions of a *bcc* lattice for the directly scattered and reflected beams, respectively. The indexed *bcc* structure has a lattice parameter, *a*, of 36.0 nm and the (110) plane parallel to the surface. The yellow line corresponds to the sample horizon, the solid red line corresponds to the critical angle of the film, and the dashed red line corresponds to the critical angle of the substrate. While block copolymer thin films typically have critical angles of ~0.1, the spot analysis shown in Figure 5.3 assumes a much smaller critical angle of 0.02. For this analysis, we propose that the block copolymer film after evaporation is composed of a two-layer structure with a solvent-swollen, self-assembled top surface above a phase separated but disordered block copolymer solution. A similar bi-layer configuration is seen in SNIPS membranes after plunging into a precipitation bath, which petrifies the kinetically trapped polymer structure.[6] In this case, the change in refractive index at the air/film interface may be fairly large, while the difference in refractive index between the self-assembled top surface and the disordered solution below would be relatively small, validating the spot assignments based on a low film critical angle.

The time-based evolution from a disordered to an ordered solution structure evident from GISAXS echoes solution SAXS of the same ISV43 system. Previous

reports of solution SAXS on both diblock copolymers and triblock terpolymers used to fabricate SNIPS membranes have shown concentration dependent ordering in selective solvent systems.[1] Figure 5.4 compares the in-plane projection of the GISAXS patterns between q_z=0.22 nm^{-1} and q_z=0.34 nm^{-1} and solution SAXS at 20 wt% and 24 wt%. The in-plane projection of GISAXS patterns at 0 s (Figure 5.4a, bottom) shows a broad peak at q_x=0.236 nm^{-1}. Similarly, solution SAXS of ISV43 at 20 wt% (Figure 5.4b, bottom), exhibits a broad peak at q=0.246 nm^{-1}. The broad peak is likely a correlation length of the phase separated disordered solution. Given that the initial concentration of the solution probed with GISAXS was 20 wt%, it is not surprising that the GISAXS after limited evaporation yields a peak position close to that observed in solution SAXS. The in-plane projection of the film after 46 of evaporation (Figure 5.4a, top) shows peaks consistent with a *bcc* structure with a primary peak position at q^*= 0.246 nm^{-1} and additional reflections at $(q/q^*)^2$=2 and 3. The corresponding lattice parameter for the bcc structure (i.e. $a = \frac{\sqrt{2} * 2\pi}{q}$) is 36.1 nm. Likewise, the solution SAXS of ISV43 at 24 wt% (Figure 5.4b, top), exhibits a scattering pattern consistent with a *bcc* morphology with a primary peak position at q^*=0.237 nm^{-1} and additional reflections at $(q/q^*)^2$=2, 3, 4, and 5. The corresponding *bcc* lattice parameter is 37.6 nm, in agreement with the morphological length scale of the evaporated GISAXS film. Overall, the structure of the film surface as observed by GISAXS is well-simulated by the solution SAXS studies.

The most intense Bragg spots are observed after an evaporation time of 46 s, however, low intensity spots first appear after 37 s and remain up to 58 s of

evaporation. At 62 s of evaporation, the GISAXS patterns exhibit diffuse rings indicating a lack of long-range order (see Appendix D, Figure D.2). This suggests a practical window of time of ~20 s in which the film can be plunged into a non-solvent and the top surface will exhibit self-assembled, periodic order.

The in-plane projection of the 46 s evaporated film (Figure 5.4a, top) exhibits an additional broad peak at q=0.212. Since this beam intensity is concentric around the reflected beam center, we speculate that the origin of this peak may be the disordered polymer solution layer below the self-assembled top layer. *In situ* GISAXS experiments in which the incident angle of the X-ray beam is varied would enable the distinction between the scattering patterns from the film substructure and the film surface structure, thus illuminating the origin of the q=0.212 peak.

While ISV43 at 20 wt% in DOX/THF (7/3 by weight) shows no ordered structure from either GISAXS or solution SAXS, it is worth noting that a 20 wt% solution in pure DOX exhibits a well-ordered structure with a primary peak position at q^*=0.234 nm^{-1} and additional reflections at $(q/q^*)^2$=2, 3, 4, 5, and 6, consistent with the *bcc* morphology (see Appendix D, Figure D.1). The replacement of 30 wt% of DOX with the less selective THF improves the solubility of the polymer, necessitating higher polymer concentrations to achieve ordered solution structure, and indicates a solvent-dependent ODT. During the evaporation of solutions in the binary solvent system, the lower boiling point THF (b.p. 66 °C) is expected to evaporate faster than the higher boiling point DOX (b.p. 101 °C) Thus, both increasing the polymer concentration and increasing amount of DOX in the solvent system drives the polymer towards self-assembly during the evaporative step in the SNIPS process.

Understanding the formation process of SNIPS membranes has important implications for broadening the scope of high-performance block copolymer membranes. Through *in situ* GISAXS on SNIPS membrane solutions, the development of a self-assembled, ordered surface structure during the formation process was demonstrated. Through this method, the key parameter of the evaporation time can be optimized through real-time observation. Such optimization can serve to improve SNIPS membrane performance by ensuring an isoporous top surface while maximizing substructure porosity.

Acknowledgement

This publication is based on work supported by award No. KUS-C1-018-02, made by King Abdullah University of Science and Technology (KAUST). R.M.D. acknowledges support from the NSF Graduate Research Fellowship Program (GRFP). This work made use of the Cornell Center for Materials Research Shared Facilities, which are supported through the NSF MRSEC program (DMR-1120296) and the Cornell High Energy Synchrotron Source (CHESS), which is supported by the NSF & NIH/NIGMS via NSF award DMR-0936384, and MacCHESS supported by NIGMS award GM-103485.

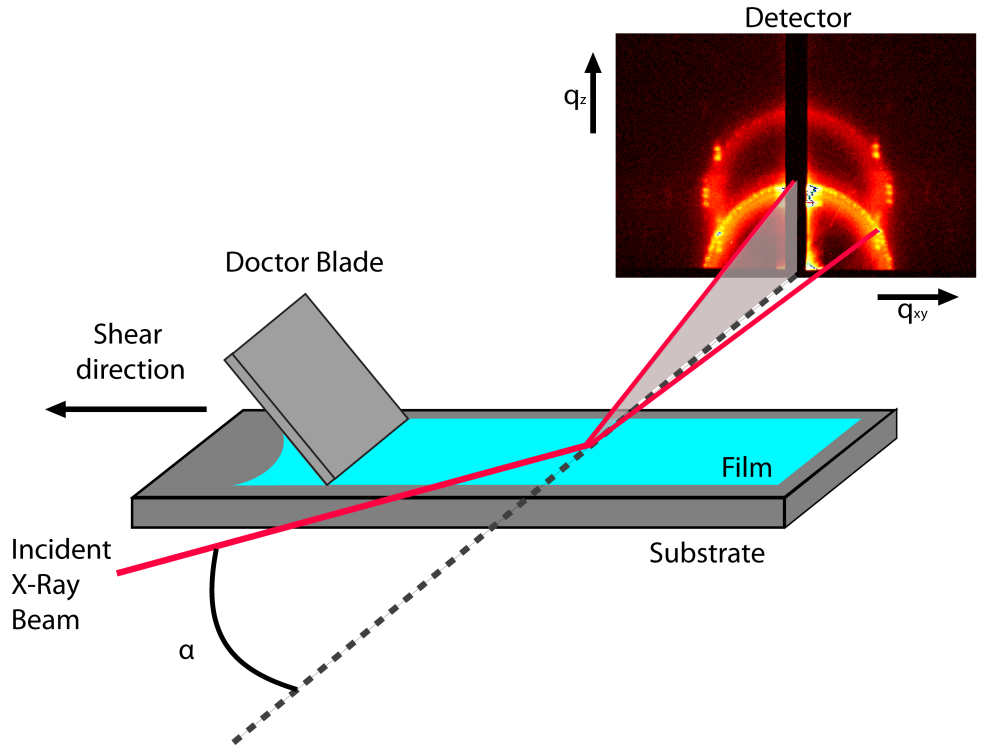

Figure 5.1 Diagram of *in situ* GISAXS experimental setup. A block copolymer solution is formed into a film using an automated doctor blade. Immediately after film formation, GISAXS patterns are collected on a CCD detector every 4-5 s.

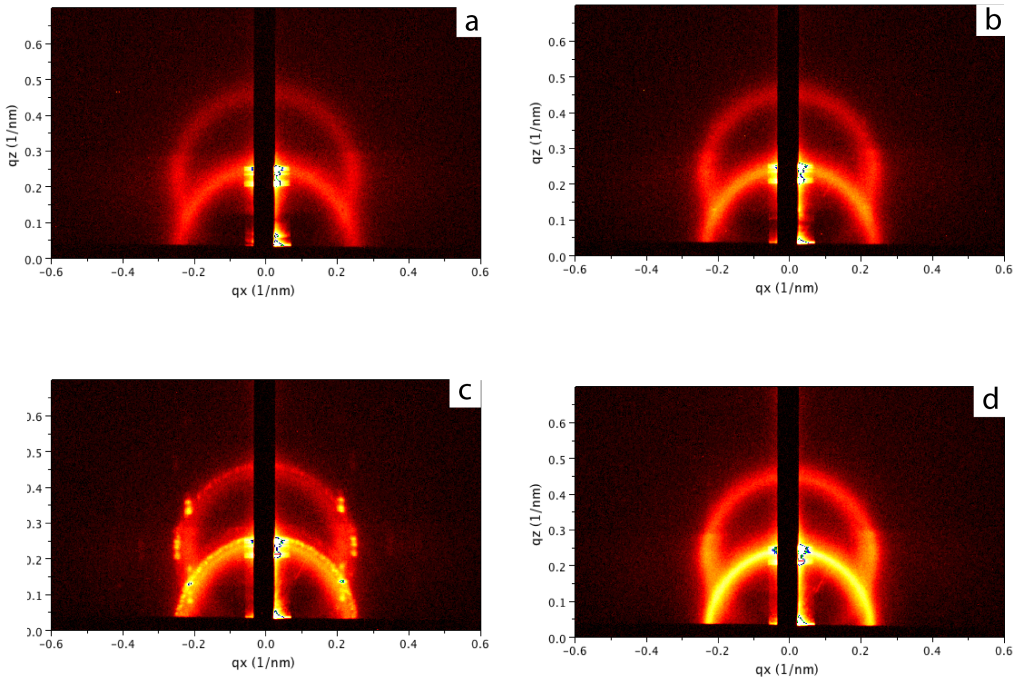

Figure 5.2. Selected GISAXS patterns of ISV terpolymer solution after various evaporation times. 0 s (a), 25 s (b), 46 s (c), and 62 s (d).

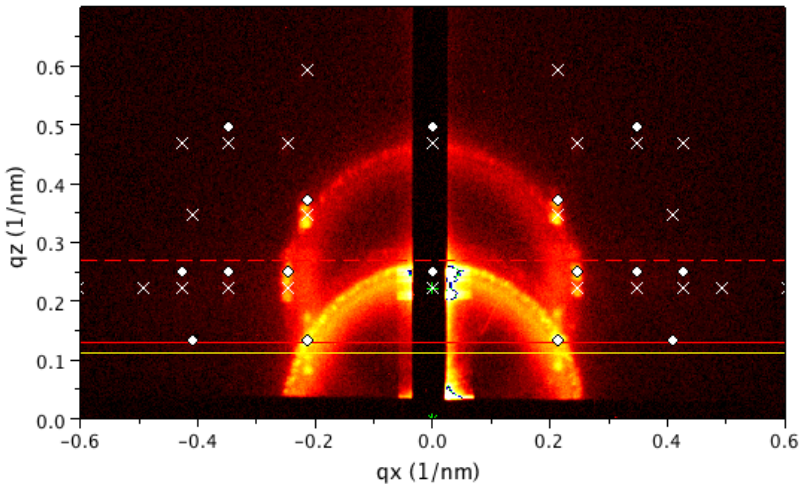

Figure 5.3. GISAXS pattern of triblock terpolymer film after 46 s of evaporation with expected spots marked for a *bcc* lattice.

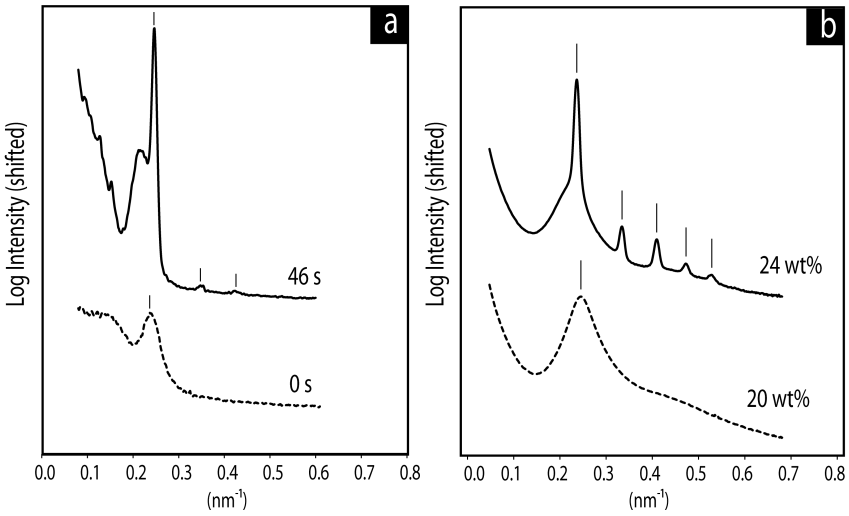

Figure 5.4 In-plane projections of selected GISAXS patterns (a) and solution SAXS (b). Tick marks correspond to either q^* or up to $(q/q^*)^2$=1, 2, 3, 4, and 5 for a *bcc* structure.

REFERENCES

1. Dorin, R. M.; Marques, D. S.; Sai, H.; Vainio, U.; Phillip, W. A.; Peinemann, K.-V.; Nunes, S. P.; Wiesner, U., Solution Small-Angle X-ray Scattering as a Screening and Predictive Tool in the Fabrication of Asymmetric Block Copolymer Membranes. *ACS Macro Letters* **2012,** *1* (5), 614-617.

2. Peinemann, K. V.; Abetz, V.; Simon, P. F., Asymmetric superstructure formed in a block copolymer via phase separation. *Nat Mater* **2007,** *6* (12), 992-6.

3. Jung, A.; Rangou, S.; Abetz, C.; Filiz, V.; Abetz, V., Structure Formation of Integral Asymmetric Composite Membranes of Polystyrene-block-Poly(2-vinylpyridine) on a Nonwoven. *Macromolecular Materials and Engineering* **2012,** *297* (8), 790-798.

4. Hahn, J.; Filiz, V.; Rangou, S.; Clodt, J.; Jung, A.; Buhr, K.; Abetz, C.; Abetz, V., Structure formation of integral-asymmetric membranes of polystyrene-block-Poly(ethylene oxide). *Journal of Polymer Science Part B: Polymer Physics* **2013,** *51* (4), 281-290.

5. Jung, A.; Filiz, V.; Rangou, S.; Buhr, K.; Merten, P.; Hahn, J.; Clodt, J.; Abetz, C.; Abetz, V., Formation of Integral Asymmetric Membranes of AB Diblock and ABC Triblock Copolymers by Phase Inversion. *Macromolecular Rapid Communications* **2013**, DOI: 10.1002/marc.201200770.

6. Phillip, W. A.; Mika Dorin, R.; Werner, J.; Hoek, E. M. V.; Wiesner, U.; Elimelech, M., Tuning Structure and Properties of Graded Triblock Terpolymer-Based Mesoporous and Hybrid Films. *Nano Letters* **2011,** *11* (7), 2892-2900.

7. Clodt, J. I.; Filiz, V.; Rangou, S.; Buhr, K.; Abetz, C.; Höche, D.; Hahn, J.; Jung, A.; Abetz, V., Double Stimuli-Responsive Isoporous Membranes via Post-Modification of pH-Sensitive Self-Assembled Diblock Copolymer Membranes. *Advanced Functional Materials* **2012,** *23* (6), 731-738.

8. Qiu, X.; Yu, H.; Karunakaran, M.; Pradeep, N.; Nunes, S. P.; Peinemann, K.-V., Selective Separation of Similarly Sized Proteins with Tunable Nanoporous Block Copolymer Membranes. *ACS Nano* **2012,** *7* (1), 768-776.

9. Nunes, S. P.; Sougrat, R.; Hooghan, B.; Anjum, D. H.; Behzad, A. R.; Zhao, L.; Pradeep, N.; Pinnau, I.; Vainio, U.; Peinemann, K.-V., Ultraporous Films with Uniform Nanochannels by Block Copolymer Micelles Assembly. *Macromolecules* **2010,** *43* (19), 8079-8085.

10. Oss-Ronen, L.; Schmidt, J.; Abetz, V.; Radulescu, A.; Cohen, Y.; Talmon, Y., Characterization of Block Copolymer Self-Assembly: From Solution to Nanoporous Membranes. *Macromolecules* **2012,** *45* (24), 9631-9642.

11. Nunes, S. P.; Karunakaran, M.; Pradeep, N.; Behzad, A. R.; Hooghan, B.; Sougrat, R.; He, H.; Peinemann, K.-V., From Micelle Supramolecular Assemblies in Selective Solvents to Isoporous Membranes. *Langmuir* **2011,** *27* (16), 10184-10190.

12. Nunes, S. P.; Behzad, A. R.; Hooghan, B.; Sougrat, R.; Karunakaran, M.; Pradeep, N.; Vainio, U.; Peinemann, K.-V., Switchable pH-Responsive Polymeric Membranes Prepared via Block Copolymer Micelle Assembly. *ACS Nano* **2011,** *5* (5), 3516-3522.

13. Paik, M. Y.; Bosworth, J. K.; Smilges, D.-M.; Schwartz, E. L.; Andre, X.; Ober, C. K., Reversible Morphology Control in Block Copolymer Films via Solvent

Vapor Processing: An in Situ GISAXS Study. *Macromolecules* **2010,** *43* (9), 4253-4260.

14. Gowd, E. B.; Bohme, M.; Stamm, M., In Situ GISAXS Study on Solvent Vapour Induced Orientation Switching in PS- b -P4VP Block Copolymer Thin Films. *IOP Conference Series: Materials Science and Engineering* **2010,** *14* (1), 012015.

15. Smilgies, D.-M.; Li, R.; Giri, G.; Chou, K. W.; Diao, Y.; Bao, Z.; Amassian, A., Look fast: Crystallization of conjugated molecules during solution shearing probed in-situ and in real time by X-ray scattering. *physica status solidi (RRL) – Rapid Research Letters* **2012,** *7* (3), 177-179.

CHAPTER 6

Outlook

The use of block copolymer self-assembly in membrane fabrication offers remarkable improvements in membrane performance over conventional polymer materials. The technique of self-assembly combined with non-solvent induced phase separation, SNIPS, potentially expands the applicability of block copolymer based membranes to large-scale applications. A particularly unique feature of SNIPS membranes is their structure control via a non-equilibrium-type process. Historically, block copolymer and hybrid materials formation has focused on the achievement of equilibrium structures that form through careful solvent or thermal annealing processes, as shown in Figure 6.1a. While this allows quantitative understanding of the resulting structures in the framework of equilibrium thermodynamics, it limits the accessible range of morphologies. In particular, it does not allow the formation of graded, asymmetric structures highly desirable in many membrane separation processes. In contrast, the SNIPS process kinetically traps a non-equilibrium based graded structure on the way to equilibrium. As demonstrated in this thesis, this can be done in a controlled manner thereby enabling the formation of previously unknown block copolymer film structures desirable in the field of ultrafiltration membranes, as shown in Figure 6.1b. Future research in the field of non-equilibrium derived SNIPS membranes may advance by targeting progress in five areas: 1) expanding the organic chemical library, 2) introducing functional, inorganic components 3) understanding formation mechanisms in specific systems, 4) demonstrating the real-world applicability via separations of relevant molecules, and 5) exploring applications

outside of separations.

Although progress has been made in the size of the SNIPS chemical library, the total number of blocks used in the SNIPS process is still in the single digits, and includes to date PS, P4VP, PI, P2VP, and PEO. All block copolymers reported for SNIPS membranes thus far have been synthesized via anionic polymerization. This is likely because this relatively specialized technique can achieve low polydispersities (PDI) (typically <1.1) and thus excellent self-assembly. However, using only block copolymers synthesized via anionic polymerization severely limits the variety of polymer chemistries available to the SNIPS process. To overcome this challenge, alternative block copolymer synthetic techniques such as controlled radical, ring-opening metathesis, group transfer, metal mediated, and immortal polymerizations, or even click chemistry can be adopted. Despite the larger PDIs observed, these techniques have all produced block copolymers that self-assemble and significantly increase the chemical choice for SNIPS membranes. In particular, new fluorinated, bioactive, high T_g, inorganic containing, chemically resistant, mechanically robust, or chemically responsive blocks would vastly enhance SNIPS membrane functionality. Furthermore, the potential simplicity and scalability of new polymerization techniques compared to ionic polymerization may be relevant in industrial applications.

The field of hybrid organic-inorganic or fully inorganic SNIPS membranes is entirely untapped and offers tremendous opportunities for advancement. Inorganic SNIPS membranes can be achieved in a variety of ways. First, fully formed organic SNIPS membranes can be post-functionalized with inorganic components. The ISV membranes described in this dissertation have been successfully post-functionalized

with silver nanoparticles and exhibit antimicrobial behavior. Unpublished work performed in the Wiesner research group has also resulted in post-functionalization of ISV SNIPS membranes via electroless plating of metals onto SNIPS templates to produce hybrid structures. Calcination of these materials resulted in fully inorganic graded-porous metal and metal oxide structures. A second method is the incorporation of inorganic components, such as sol gels, nanoparticles, or inorganic precursors, directly into the casting solution. This method will result in as-made hybrid materials, but may face challenges such as disruptions in block copolymer self-assembly, weak interactions between organic and inorganic components, and low inorganic loadings. A third method is the direct incorporation of inorganic building blocks into the block copolymer, e.g. polysilsesquioxanes, which can subsequently be transformed into a ceramic material through a post-formation heating process.

Advancements in the field of SNIPS membranes may necessarily rely on a thorough understanding of formation mechanisms. Most studies have concluded that casting solutions contain micelles.[1-5] For the most well-studied PS-*b*-P4VP system, however, discrepancies in proposed micelle structure and formation mechanism remain unresolved. The ISV SNIPS membranes detailed in this dissertation may form through a pathway distinct from that of the diblock, which is supported by the longer evaporation times used, the different pore geometry observed, and the lower pore surface area. The micelle structure in the ISV triblock system is suggested to have the PI block at the core and the P4VP block on the surface, as evidenced by TEM cross sections of the membrane and suggested by solubility parameters.[5] Small-angle neutron scattering on the ISV casting solutions would provide direct evidence of

micelle structure and may further clarify the formation mechanism. While such mechanistic studies are challenging, detailed understanding of the membrane formation mechanism may open the door to successful translation of a larger variety of block copolymer chemistries as well as mesoscopic morphologies to the SNIPS membrane structure.

Many of the studies performed in research labs worldwide garner significant interest and attract resources when real-world applicability is demonstrated. SNIPS membranes represent a long-needed advancement in membranes for separation applications used in industries from water treatment to dialysis. As such, the use of SNIPS membranes under conditions relevant to industrial separations would propel this field forward. Both the model protein bovine serum albumin (BSA) and synthetic PEO have been used to show rejection in SNIPS membranes. Most recently, post-functionalized PS-*b*-P4VP SNIPS membranes have been used to selectively separate the similarly sized BSA from bovine hemoglobin (BHb) in diffusion experiments.[6] The next step is to perform similar separations under pressures, flow rates, and feed volumes necessary for industrial processes.

Finally, a largely unexplored aspect of SNIPS membranes is their use in applications outside of separations science. For example, membranes that have P4VP on the surface exhibit pH dependent fluxes, effectively closing off the pores at a pH below the pK_a of P4VP (~4.6).[7] Such behavior may serve as a chemical valve in, e.g., microfluidic devices. The membranes also exhibit a hierarchical structure with pores that span from ~10 nanometers to ~10 microns. These high surface area materials would be suitable as a catalyst support, and may be useful in the transport of electrons

or fuels. Inorganic, conductive SNIPS membranes may be applicable, for example, as fuel cell electrodes in which the surface is decorated with catalysts and the pores are infiltrated with a proton conductor. Such a construction may improve efficiency by shrinking the distance between active sites and reducing ion transport resistance. The small list of applications outside of separations described here is by no means exhaustive, and the unique non-equilibrium structure of SNIPS membranes may be useful as sensors, drug delivery systems, and beyond.

Developing and understanding SNIPS membranes is an interdisciplinary process that encompasses polymer chemistry, materials science, biology, and much more. This feature requires the collaborative efforts of experts from a variety of fields and perspectives, and may thrive in particular at organizations that can interface such fields. The field of SNIPS, conceived less than a decade ago, promises enormous potential in the coming years.

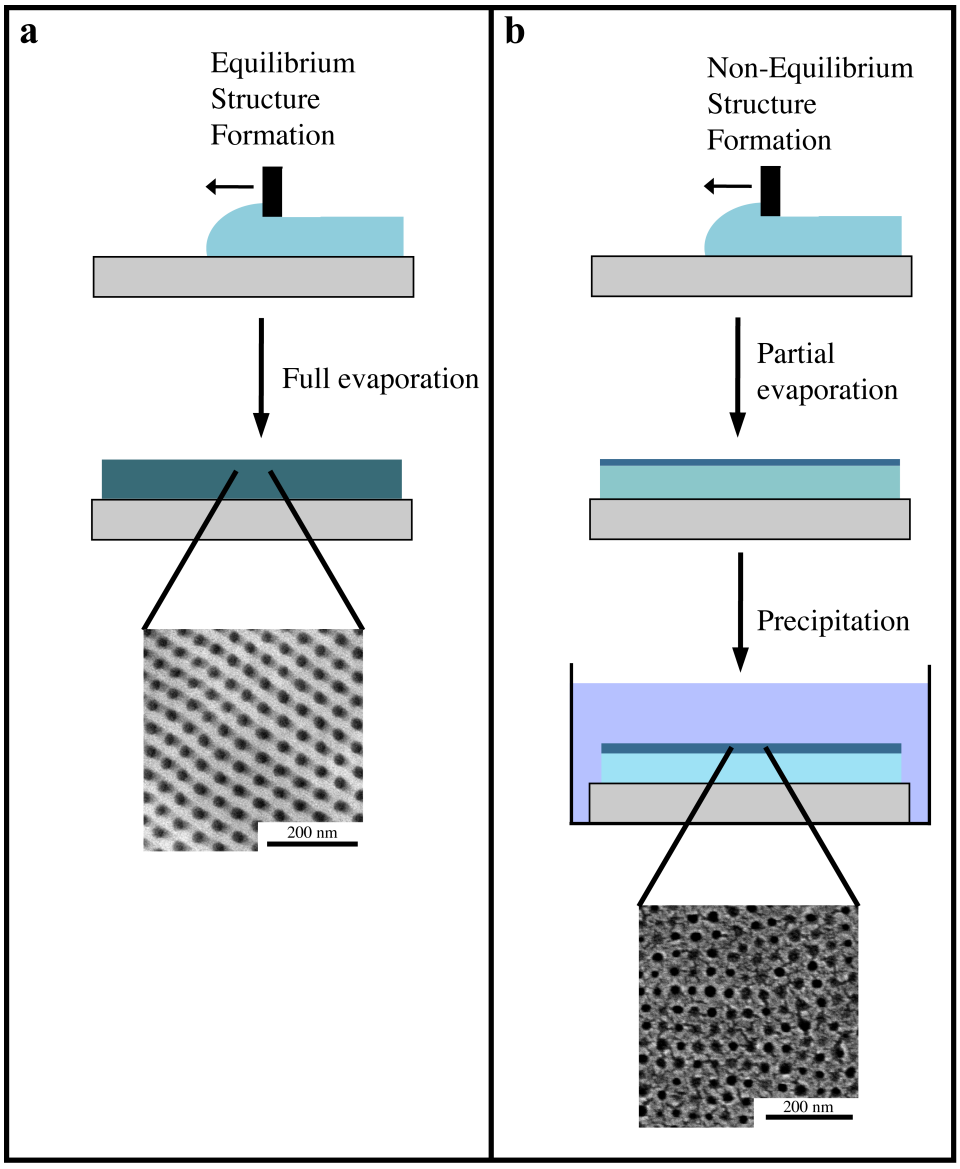

Figure 6.1 Equilibrium versus non-equilibrium structure formation in block copolymer systems. Doctor bladed solutions showing equilibrium bulk structure after full evaporation (a), and non-equilibrium structure after partial evaporation and precipitation (b).

REFERENCES

1. Nunes, S. P.; Behzad, A. R.; Hooghan, B.; Sougrat, R.; Karunakaran, M.; Pradeep, N.; Vainio, U.; Peinemann, K.-V., Switchable pH-Responsive Polymeric Membranes Prepared via Block Copolymer Micelle Assembly. *ACS Nano* **2011,** *5* (5), 3516-3522.

2. Nunes, S. P.; Karunakaran, M.; Pradeep, N.; Behzad, A. R.; Hooghan, B.; Sougrat, R.; He, H.; Peinemann, K.-V., From Micelle Supramolecular Assemblies in Selective Solvents to Isoporous Membranes. *Langmuir* **2011,** *27* (16), 10184-10190.

3. Dorin, R. M.; Marques, D. S.; Sai, H.; Vainio, U.; Phillip, W. A.; Peinemann, K.-V.; Nunes, S. P.; Wiesner, U., Solution Small-Angle X-ray Scattering as a Screening and Predictive Tool in the Fabrication of Asymmetric Block Copolymer Membranes. *ACS Macro Letters* **2012,** *1* (5), 614-617.

4. Oss-Ronen, L.; Schmidt, J.; Abetz, V.; Radulescu, A.; Cohen, Y.; Talmon, Y., Characterization of Block Copolymer Self-Assembly: From Solution to Nanoporous Membranes. *Macromolecules* **2012,** *45* (24), 9631-9642.

5. Phillip, W. A.; Mika Dorin, R.; Werner, J.; Hoek, E. M. V.; Wiesner, U.; Elimelech, M., Tuning Structure and Properties of Graded Triblock Terpolymer-Based Mesoporous and Hybrid Films. *Nano Letters* **2011,** *11* (7), 2892-2900.

6. Qiu, X.; Yu, H.; Karunakaran, M.; Pradeep, N.; Nunes, S. P.; Peinemann, K.-V., Selective Separation of Similarly Sized Proteins with Tunable Nanoporous Block Copolymer Membranes. *ACS Nano* **2012,** *7* (1), 768-776.

7. Mika, A. M.; Childs, R. F., Acid/base properties of poly(4-vinylpyridine)

anchored within microporous membranes. *Journal of Membrane Science* **1999,** *152* (1), 129-140.

APPENDIX A

Poly(isoprene-*b*-styrene-*b*-4-vinylpyridine) synthesis

The poly(isoprene-*b*-styrene-*b*-4-vinylpyridine) triblock terpolymer used in this study was synthesized using a sequential anionic polymerization technique. The concentration of the polymer was kept under 10 wt % throughout the procedure. ~500 mL of benzene was distilled into a 1 L reactor and the anionic initiator *sec*-BuLi was added to the reactor in a glove box via syringe. Distilled isoprene was added to the reactor and allowed to polymerize for a minimum of 8 hours before a 5 mL aliquot was terminated with methanol for GPC analysis. Distilled styrene was then added to the reactor in the glove box via syringe. The styrene polymerized onto the polyisoprene block for 36 h, after which a small aliquot was terminated with methanol for GPC and NMR analysis. The benzene was subsequently removed from the reactor and a 10× molar excess of diphenylethylene (DPE) was added relative to the *sec*-BuLi. Approximately 500 mL of THF was distilled directly into the reactor, which was then cooled to -78 °C and distilled 4-vinylpyridine was added. The 4-vinylpyridine polymerized onto the poly(isoprene-*b*-styrene) for 1.5 h, after which the triblock terpolymer was terminated with degassed methanol. The final terpolymer was dissolved in chloroform and twice precipitated into methanol.

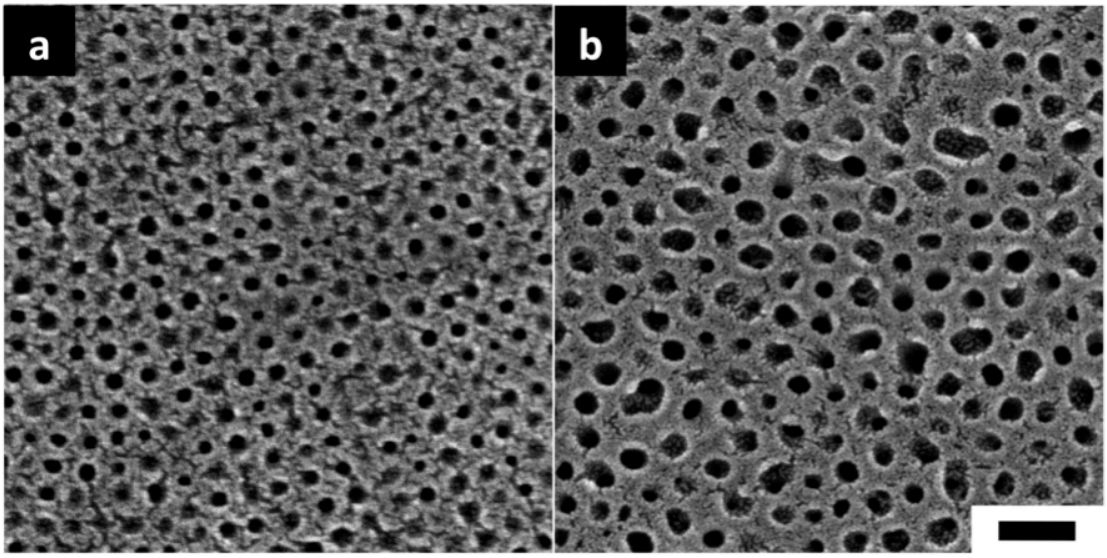

Figure A.1 SEM micrographs of the top surface of mesoporous films a. Top surface of a parent ISV-77 film. **b.** Top surface of a hybrid ISV-77 film. Visual comparison of the parent and hybrid films indicates that the blended homopolymer P4VP increases the pore size, consistent with observed transport behavior. The scale is the same for both images with scale bar of 100 nm.

APPENDIX B

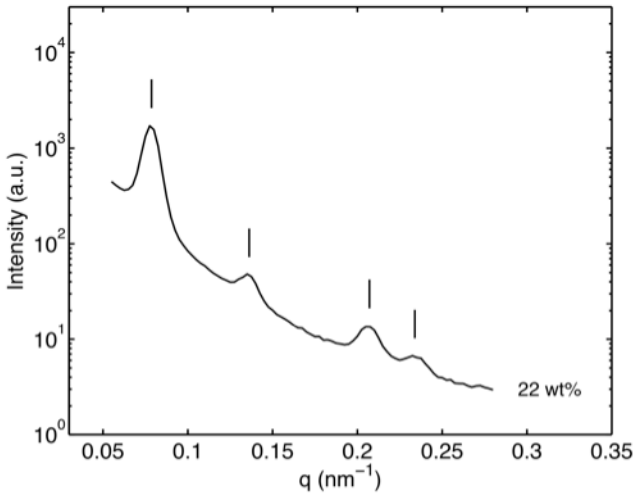

Figure B.1 Small-angle x-ray scattering curve for SV-240 in 1/1/1 DOX/THF/DMF by weight at 22 wt%. Dash markings in correspond to (q/q^*)2=1, 3, 7, and 9 consistent with a 2D hexagonal lattice.

APPENDIX C

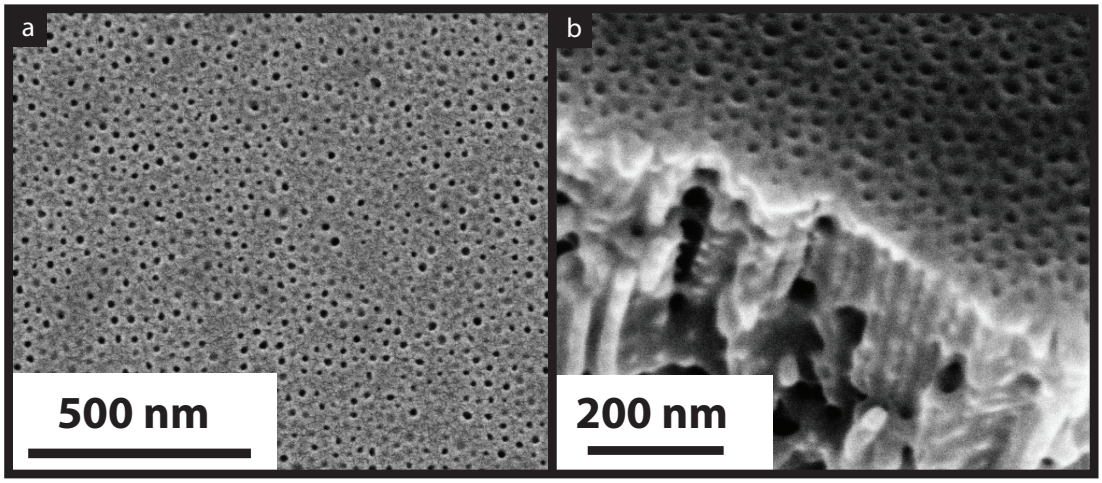

Figure C.1 SEM micrograph of the top surface (a) and cross section (b) of ISV115 membrane cast from a 9 wt% 7/3 DOX/THF casting solution evaporated for 75 s.

APPENDIX D

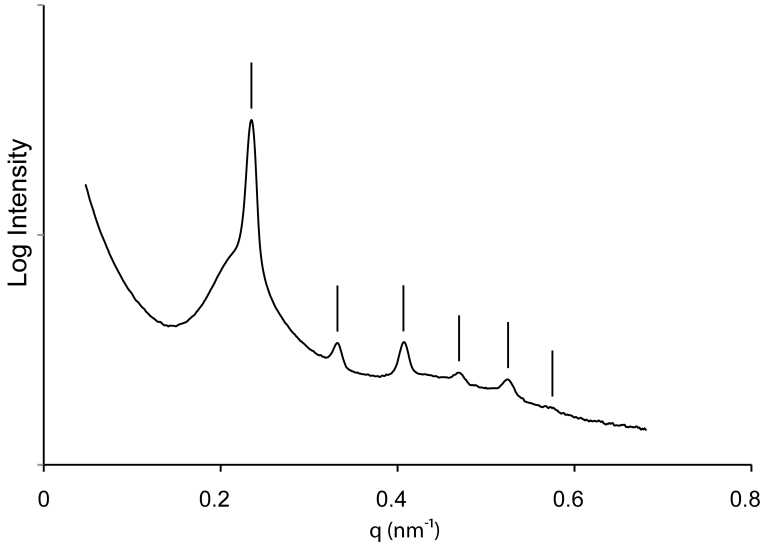

Figure D.1 Solution SAXS of ISV43 at 20 wt% in a solution of pure 1,4-dioxane. A primary peak position at q=0.235 nm^{-1} and additional reflections marked at $(q/q^*)^2$=2, 3, 4, 5, and 6 consistent with a *bcc* lattice are observed. A lattice spacing, a, of 37.8 nm can be calculated from the primary peak position.

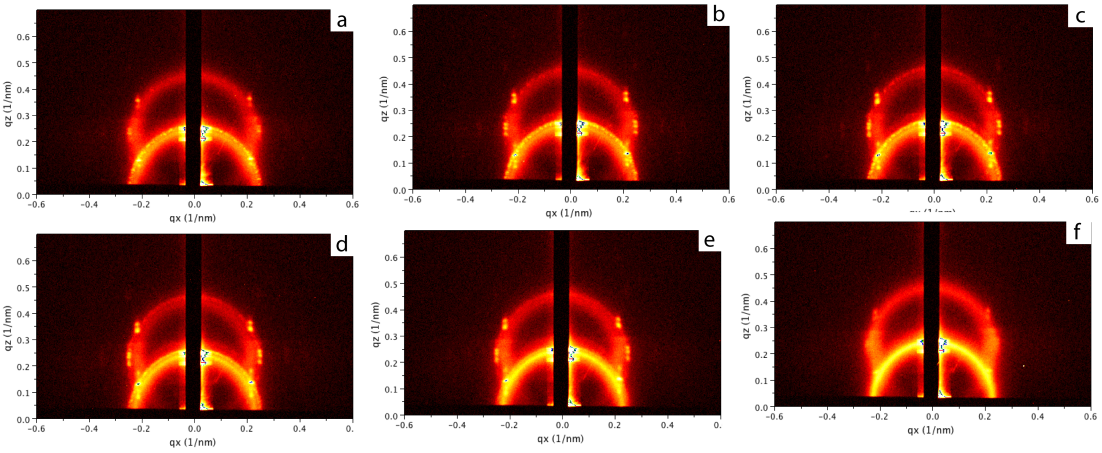

Figure D.2 GISAXS patterns from ISV43 films exhibiting Bragg spots consistent with a *bcc* lattice evaporated at 37 s (a), 41 (b), 46 s (c), 50 s (d), and 54 s (e), and 58 s (f).